Spring 2018

Cyclic axial compression behavior of concrete-filled hybrid large rupture strain FRP tubes

Monika Nain

Department:

CYCLIC AXIAL COMPRESSION BEHAVIOR OF CONCRETE-FILLED HYBRID LARGE RUPTURE STRAIN FRP TUBES

by

MONIKA NAIN

A THESIS

Presented to the Faculty of the Graduate School of the

MISSOURI UNIVERSITY OF SCIENCE AND TECHNOLOGY

In Partial Fulfillment of the Requirements for the Degree

MASTER OF SCIENCE

in

CIVIL ENGINEERING

2018

Approved by

Mohamed A. ElGawady, Advisor
Guirong Grace Yan
John Myers

PUBLICATION THESIS OPTION

This thesis consists of the following two articles, formatted in the style used by the Missouri University of Science and Technology.

Paper I: Pages 4-44 is a manuscript entitled “Cyclic Axial Compression Behavior of Concrete-Filled Hybrid Large Rupture Strain FRP Tubes” This manuscript will be submitted for publication in the in the *Journal of Structural Engineering* published by the American Society of Civil Engineers (ASCE), and the Journal of ACI special publication published by American Concrete Institute (ACI).

Paper II: Pages 45-76 is a manuscript entitled “Behavior of Concrete-Filled Hybrid Small and Large Rupture Strain FRP Tubes under Cyclic Axial Compression” This manuscript will be submitted for publication in the in the *Journal of Structural Engineering* published by the American Society of Civil Engineers (ASCE), and the Journal of ACI special publication published by American Concrete Institute (ACI).

ABSTRACT

This study introduces an experimental investigation of the behavior of concrete filled fiber reinforced polymer (FRP) tubes (CFFTs) under cyclic axial compression. The FRP used in this study were either small rupture strain FRP (SRS-FRP) or large rupture strain FRP (LRS-FRP). This paper also presents the first-ever experimental study on the behavior of concrete confined using hybrid LRS-FRP and SRS-FRP. LRS-FRP included PEN (polyethylene napthalate) and PET (polyethylene terephthalate) where both of them having ultimate axial strain larger than 5%, and low stiffness. SRP-FRP included carbon and glass FRP having small rupture strains, smaller than 2%, and high stiffness. The behavior of CFFTs having different confinement ratios were investigated in terms of ductility, ultimate strain, confinement effectiveness, and energy dissipation capacity. The results revealed that LRS-FRP showed highly ductile behavior and significant energy dissipation capacity with the same strength enhancement as of SRS-FRP. Furthermore, using the hybrid CFFTs remarkably improved the ductility and energy dissipation capacity of SRS-CFFTs.

ACKNOWLEDGMENTS

I would like to express my deep gratitude and sincere thanks to my advisor, Dr. Mohamed ElGawady. The idea of the work presented in this thesis is developed by Dr. ElGawady. His guidance and close mentoring throughout executing this research was crucial for completing this thesis. I would also like to thank the members of my advisory committee, Dr. Grace Yan and Dr. John Myers.

I would also like to acknowledge my fellow researcher Mohanad Abdulazeez. The experimental and analytical work presented in this thesis is carried out by me and Mohanad Abdulaziz helped me during preparing the test specimens and discussion of the test results. I would also thank my research team Ahmed Gheni, Song Wang, and Nicholas Colbert for helping me in the research. I would like to thank Civil Engineering Department staff: Gary Abbot, John Bullock, Brian Swift, and Greg Leckrone for their kind assistance throughout the research

I want to express my gratitude and deepest appreciation to my family. To my parents, Dr. Rajender Singh and Mrs. Kamlesh Nain, who has supported and encouraged me all the time.

TABLE OF CONTENTS

Page

LIST OF ILLUSTRATIONS

Paper I Page

LIST OF TABLES

SECTION

1. INTRODUCTION

1.1 BACKGROUND

In the past few decades, rapid growth has been observed in the applications of FRP confinement for new construction and strengthening/retrofitting of reinforced concrete elements. Application of FRP confinement instead of steel is preferable due to easy installation, high strength to weight-ratio, corrosion resistance, and relatively low maintenance cost. Concrete filled fiber reinforced polymer (FRP) tubes (CFFTs) has proven to be able to increase the strength and ductility of the structures. It consists of outer FRP tube filled with plain concrete inside, where FRP provides lateral confinement during axial compression.

Carbon and glass are the most common fibers used commercially for manufacturing FRP having rupture strain of around 2%. Many studies have proven their application in strength enhancement of structure elements. However, due to small rupture strain (SRS) of these FRPs their application is limited in seismic areas as the SRS-CFFT does not provide ductility. In recent years, a new category of FRP has emerged as an alternative to SRS-FRPs called large rupture strain FRPs (LRS-FRP). Owing to large rupture strain property of LRS-FRP, CFFT shows higher ductile behavior which can be an efficient system in seismic areas. LRS-FRP include PEN (polyethylene napthalate) and PET (polyethylene terephthalate) with rupture strain of more than 5%. Moreover, PEN and PET are cheaper and environment-friendly, since they are produced using recycled material, than SRS-FRP.

Although a large number of studies has been done on SRS-CFFTs, significantly less studies were carried out to understand the behavior of LRS-CFFTs. Moreover, while a confined element would be subjected to cyclic reversed strains during an earthquake, relatively a limited number of studies investigated the axial cyclic load behavior of LRS-FRP confined concrete. Hence, this paper investigates experimentally the performance of CFFTs with varying confinement ratio under cyclic axial compressive loading. The performance of CFFTs is studied in terms of strength enhancement, ductility, and energy dissipation capacity.

1.2. THESIS ORGANIZATION

This thesis was organized into two sections. In Section 1, the background of concrete-filled FRP tubes and previous studies were discussed along with objective of the research. Two jounal papers were also included in Section 1.

In Paper I, the cyclic axial compression behavior of concrete- filled FRP tubes (CFFTs) was discussed. This study was performed for LRS-CFFTs, SRS-CFFTs and Hybrid LRS-SRS-CFFTs. Test results were discussed in terms of strength, ductility, confinement pressure, dilation properties and energy dissipation capacity. Strength evaluation using existing models and statistical results of this study were also discussed.

In Paper II, the behavior of CFFT under cyclic axial compression loading was discussed. In this study, a different type of SRS-FRP i.e. Carbon-FRP and LRS-FRP was used to study the behavior of CFFT. The performance of CFFTs is studied in terms of strength enhancement, ductility, and energy dissipation capacity.

Section 2 concludes the summary and findings of the above-mentioned papers. Section 2 also recommend work for future research.

1.3. OBJECTIVES

The research on cyclic axial compression behavior for LRS-CFFT was limited. Moreover, no experimental study has been conducted on hybrid LRS-SRS CFFTs. This research study was conducted to understand the behavior of CFFTs under cyclic axial compression behavior.

For the first part, CFFTs with varying confinement ratios were tested under cyclic axial compression loading. Types of FRP used in this study were: PET-FRP and PEN-FRP categorized as LRS-FRP, and Glass-FRP categorized as SRS-FRP. Test results will be discussed to better under the behavior of CFFTs.

For the second part, experimental study for different types of FRP: LRS-FRP (PET AND PEN-FRP), and SRS-FRP (Carbon-FRP) was conducted. Strength enhancement, ductility, and energy dissipation capacity will be studied. Evaluation of strength obtained from the existing models and tested results with also be done.

PAPER

I. CYCLIC AXIAL COMPRESSION BEHAVIOR OF CONCRETE-FILLED HYBRID LARGE RUPTURE STRAIN FRP TUBES

Monika Nain[1]; Mohanad M. Abdulazeez[2], S.M.ASCE; and Mohamed A. ElGawady[3§], Ph.D., M. ASCE

ABSTRACT

This paper experimentally investigates the behavior of concrete filled fiber reinforced polymer (FRP) tubes (CFFTs) under cyclic axial compression. The FRP used in this study were either small rupture strain FRP (SRS-FRP), large rupture strain FRP (LRS-FRP) or hybrid LRS-FRP and SRS-FRP. LRS-FRP are manufactured out of polyethylene naphthalate (PEN) and polyethylene terephthalate (PET) obtained from recycled plastics. Hence, they are much cheaper and environment-friendly than SRS-FRP i.e. glass FRP (GFRP) or carbon FRP (CFRP). LRS-FRP has high tensile rupture strain (usually greater than 5%) compared to 1-2% for GFRP and CFRP. This study presents the results of seventeen cylinders having different confinement ratios to investigate the behavior of concrete filled LRS-FRP, hybrid LRS-FRP, and GFRP tubes in terms of ductility, ultimate strain, strength improvement, and energy dissipation. A comparison has been conducted between the attained experimental results and existing analytical models in this study. The

[1]Graduate Research Assistance, Dept. of Civil, Architectural, and Environmental Engineering, Missouri University of Science and Technology, Rolla, MO. 65409; mnb94@mst.edu
[2]Graduate Research Assistance and PhD student, Dept. of Civil, Architectural, and Environmental Engineering, Missouri University of Science and Technology, Rolla, MO. 65409; mma548@mst.edu
[3] Benavides Associate Professor, Dept. of Civil, Architectural, and Environmental Engineering, Missouri University of Science and Technology, Rolla, MO. 65409; elgawadym@mst.edu
[§]Corresponding author

results showed that using LRS-FRP significantly improved the ductility and ultimate strength of the confined concrete. The hybrid confinement improves the ductility and energy dissipation capacity of the concrete.

1. INTRODUCTION

Fiber reinforced polymer (FRP) is a promising material in structural engineering applications because of its high strength, easy installation, corrosion resistance, and lightweight nature. Both the strength and the ductility of concrete members can be increased by using the appropriate amount of FRP confinement. In the past few decades, rapid growth has been observed in the applications of FRP confinement for new construction and strengthening/retrofitting of reinforced concrete elements (Abdelkarim and ElGawady 2014; Abdelkarim et al. 2016; Abdulazeez 2017; Abdulazeez et al. 2017; Fam and Rizkalla 2001; Fam and Rizkalla 2002; Lam and Teng 2001; Mirmiran and Shahawy 1997; Mirmiran et al. 1998; Moustafa and ElGawady 2016; Ozbakkaloglu 2013; Ozbakkaloglu and Akin 2011; Ozbakkaloglu and Oehlers 2008; Saleem et al. 2016; Youssf et al. 2014).

Carbon and glass are the most common fibers used commercially for manufacturing FRP. However, these FRP suffered from small rupture strain (SRS). In recent years, polyethylene naphthalate (PEN) and polyethylene terephthalate (PET)-FRP have emerged as alternatives to SRS-FRP with large rupture strain (LRS) of more than 5% (Abdelkarim and ElGawady 2014; Abdelkarim et al. 2016; Fam and Rizkalla 2001; Fam and Rizkalla 2002; Lam and Teng 2001; Mirmiran and Shahawy 1997; Mirmiran et al. 1998; Moustafa and ElGawady 2016; Ozbakkaloglu 2013; Ozbakkaloglu and Akin 2011; Ozbakkaloglu

and Oehlers 2008; Saleem et al. 2016; Youssf et al. 2014). Furthermore, PEN and PET are cheaper and environment-friendly, since they are produced using recycled material, than conventional fiber.

Few studies were carried out to understand the behavior of LRS-FRP confined concrete and compared their behavior to SRS-FRP confined concrete (Anggawidjaja et al. 2006; Dai et al. 2011; Dai and Bai 2014). These studies showed that LRS-CFFTs, despite having low stiffness, could efficiently improve the ductility of confined concrete elements. At the ultimate state, the large strain of FRP allows the fiber composite to contribute enough force while avoiding fiber rupture and thereby improves the ductility (Dai and Bai 2014). Similar to SRS-FRP-confined concrete, Moon (2012) also reported that the LRS-FRP-confined concrete's response increases almost linearly with the increase in the number of layers of FRP. Abdelkarim and ElGawady (2015) were the first to numerically investigate the performance of hybrid LRS-SRS-FRP confined concrete. The study showed the outstanding performance of LRS-SRS FRP confined concrete in terms of ductility, deformation capacity, and energy dissipation capacity.

2. RESEARCH SIGNIFICANCE

Although a numerous number of studies has been carried out on SRS-FRP, significantly less amount of work was carried out on the LRS-FRP. Furthermore, while a confined element would be subjected to cyclic reversed strains during an earthquake, relatively a limited number of studies investigated the axial cyclic load behavior of LRS-FRP confined concrete (Bai et al. 2013; Bai 2014; Jirawattanasomkul et al. 2013; Rousakis

2013). Hence, this paper investigates experimentally the performance of concrete-filled LRS-FRP and hybrid LRS-SRS-FRP cylinders under cyclic axial compressive loading.

This study includes investigating the effects of the confinement ratio, wrapping sequence, and types of fiber (LRS, SRS, LRS-SRS) on the behavior of CFFTs to provide a better understanding of LRS-FRP confined concrete in terms of strength, rupture strain, ductility, and energy dissipation. Finally, the obtained results in term of the confined strength were compared with the available confinement models.

3. EXPERIMENTAL WORKS

Seventeen CFFTs' cylinders (Fig. 1), each cylinder having a dimension of 156 mm x 305 mm (6-inch x 12-inch), were tested under static cyclic axial compression during this study. The main variables were the confinement ratio (CR) define per equation 1 and the different types of fibers (Fig. 2 and Table 1).

$$CR = \frac{f_l}{f'_c} \tag{1}$$

$$f_l = {}^{2E_f \varepsilon_f t_f}\Big/_{D_f} \tag{2}$$

where f_l is the confining pressure, f'_c is the compressive strength of unconfined concrete, E_f is the FRP axial modulus of elasticity, t_f is the total thickness of the FRP tube, ε_f is the axial ultimate tensile strain of the FRP, and D_f is the internal diameter of the FRP tube.

The CFFT specimens were divided into three groups based on the used-fiber type: concrete filled SRS fiber tubes (SRS-CFFT), concrete filled LRS fiber tubes (LRS-CFFT), and concrete-filled hybrid fiber tubes (H-CFFT). The LRS-CFFT group had six cylinders P1 through P6 using only either PET (PET-CFFT) or PEN (PEN-CFFT) fibers with a

different number of plies ranging from one to three. The SRS-CFFT had three cylinders P7 through P9 using glass FRP with a different number of plies ranging from one to three.

The H-CFFT group had eight cylinders P10 through P17 with different combinations of three plies of LRS-FRP and SRS-FRP (Table 1). Two FRP sequences were used: either LRS-FRP was wrapped first followed by wrapping the SRS-FRP or vice versa. The former is designated as #PEN-#GFRP-CFFTs or #PET-#GFRP-CFFTs. While the later is designated as #GFRP-#PEN-CFFTs or #GFRP-#PET-CFFTs where # stand for the number of layers of FRP used.

3.1. FRP TUBES PREPARATION

The FRP tubes were made by manual wet lay-up of FRP plies wrapped around a Sonotube using an epoxy resin. The required numbers of FRP layers were continuously wrapped around the Sonotube and the last FRP layer had an overlap length of 30% of the

Fig. 1: CFFT specimens before testing

Fig. 2: Types of FRP used in the experiment (a) Glass, (b) PET, and (c) PEN

tube perimeter in the circumferential direction. Two components of epoxy, namely A and B, were mixed for 5 mins and then fiber was made fully saturated with epoxy using a roller. FRP was wrapped around the Sonotube according to the required number of plies, and then additional epoxy was applied as an overcoat to ensure enough wetting of the FRP. After curing, Sonotube was removed and hollow FRP tube was produced. The prepared CFFT specimens had confinement ratios ranging from 0.15 to 0.58 (Table 1).

Once the FRP tubes were manufactured they were left to cure at ambient temperature 24°C (76°F) in the laboratory for 7 days; then, concrete was poured into the tubes and left to cure in the laboratory at ambient temperature 24°C (76°F) for 28-days.

3.2. FRP PROPERTIES

The properties of PET-FRP, PEN-FRP, and GFRP were determined from coupon tensile tests according to ASTM D3039 (Table 2). Three coupons of each type of FRP were prepared with a different number of plies ranging from one to three. Each coupon was 254 mm (10 inches) in length and 25.4 mm (1 inch) in width

Table 1: Summary of the tested cylinders

	Cylinder label	FRP type	FRP plies #			Total FRP plies thickness [mm (inch)]	Confinement ratio (CR)
			PET	PEN	GFRP		
LRS-CFFT	P1	PET	1	-	-	3.3 (0.13)	0.15
	P2		2	-	-	6.6 (0.26)	0.29
	P3		3	-	-	9.9 (0.39)	0.44
	P4	PEN	-	1	-	3.0 (0.12)	0.19
	P5		-	2	-	6.0 (0.24)	0.37
	P6		-	3	-	9.1 (0.36)	0.56
SRS-CFFT	P7	Glass	-	-	1	1.27 (0.05)	0.19
	P8		-	-	2	2.54 (0.1)	0.39
	P9		-	-	3	3.81 (0.15)	0.58
H-CFFT	P10	PET-Glass (in/out)	2	-	1	7.87 (0.31)	0.49
	P11		1	-	2	5.84 (0.23)	0.53
	P12	PEN-Glass (in/out)	-	2	1	7.27 (0.29)	0.57
	P13		-	1	2	5.54 (0.22)	0.57
	P14	Glass-PET (in/out)	1	-	2	5.84 (0.23)	0.53
	P15		2	-	1	7.87 (0.31)	0.49
	P16	Glass-PEN (in/out)	-	1	2	5.54 (0.22)	0.57
	P17		-	2	1	7.27 (0.29)	0.57

These coupons were cut from FRP plates that were made by manual wet lay-up following the same procedure that was used for manufacturing the FRP tubes (Fig. 3). The plates were left to cure at laboratory ambient temperature for one week before cutting the coupons with required dimensions. Aluminum tabs were bonded at the two ends of each FRP coupons before the tensile tests to ensure uniform stress distribution during the tensile testing as well as to minimize stress concentrations near the gripping zone (Fig. 3).

Two strain gauges were attached to the middle of each coupon to measure the longitudinal and transverse strains. A clip gauge were also attached to the middle 127 mm (5 inch) to measure the axial strain. The specimens were tested using MTS 880 and a loading rate of 12.7 mm/min. (0.5 inches/min).

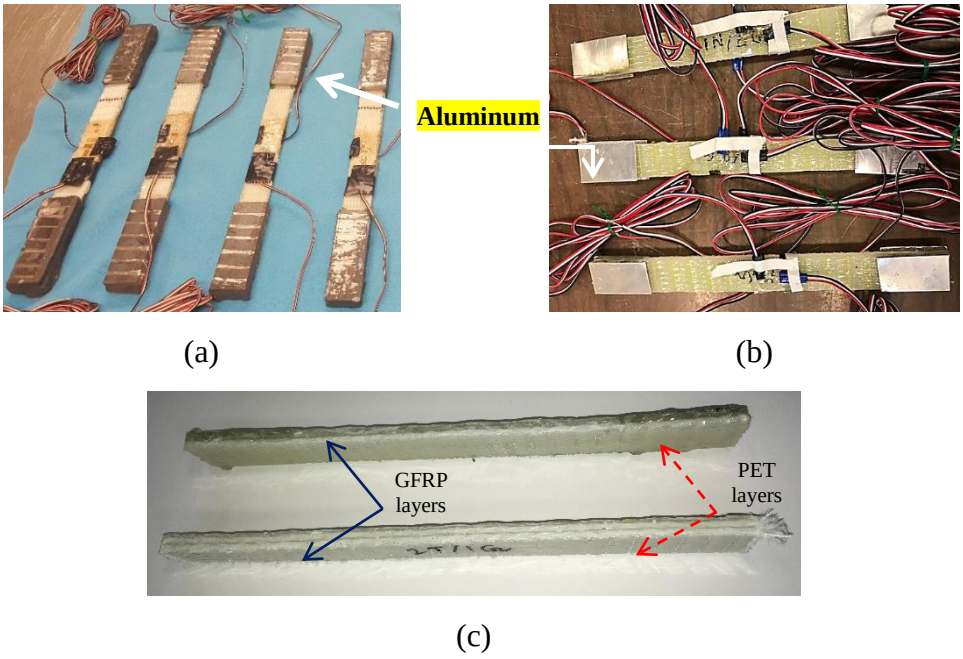

Fig. 3: FRP coupons (a) PET, (b) hybrid, and (c) hybrid coupons close up view

The LRS-FRP coupons show bilinear stress-strain relationship (Fig. 4) and failure was due to longitudinal slippage between fibers at the middle section whereas the SRS-FRP coupons show linear stress-strain relationship up to rupture (Fig. 4) and failure was due to rupture of the FRP at mid-height. Table 2 and Fig. 4 show the two different values of elastic modulus for LRS-FRP coupons, namely the initial elastic modulus (E_1) and post elastic modulus (E_2).

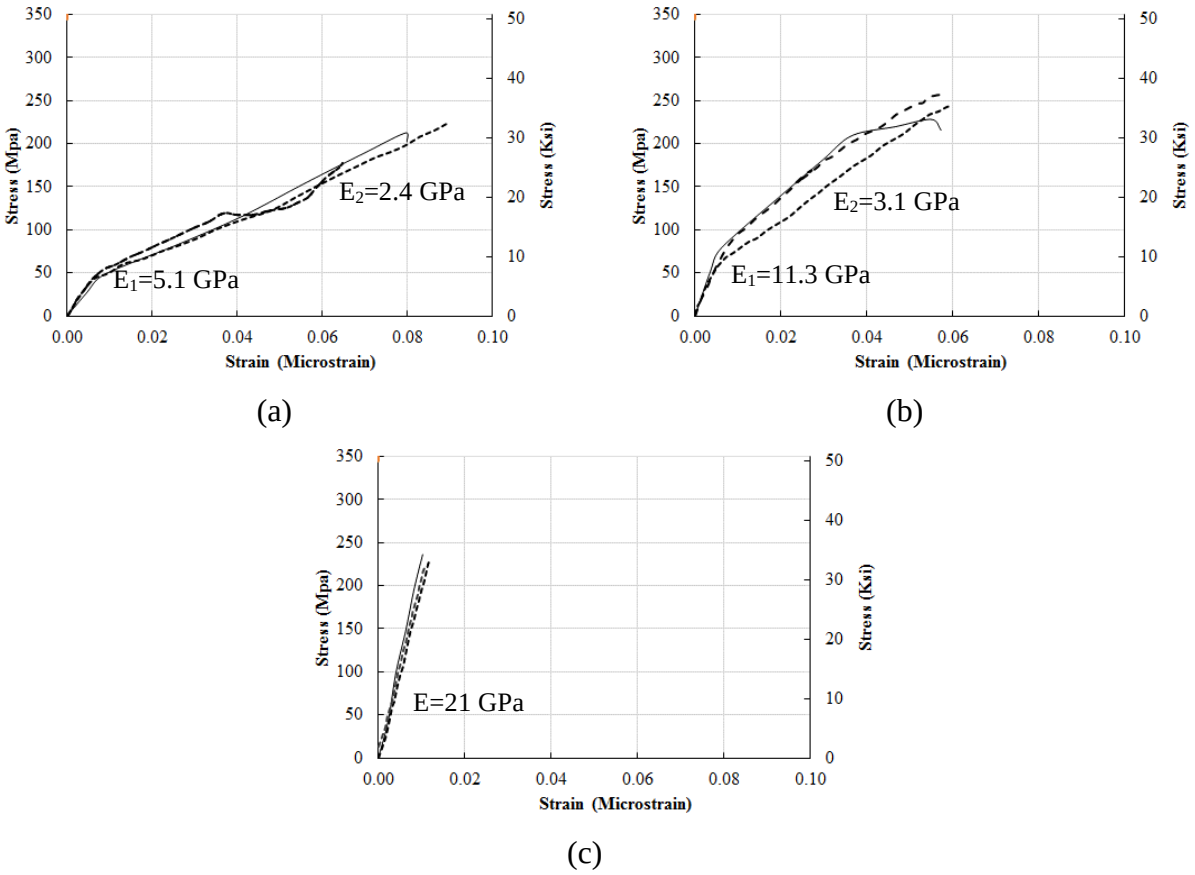

Fig. 4: FRP three coupons tensile test results (a) PET, (b) PEN, and (c) GFRP

Table 2: Properties of the used FRP

Properties	Glass	PET	PEN
Thickness/ply [mm (inch)]	1.27 (0.05)	3.3 (0.13)	3.0 (0.12)
E_1 /E_2 [GPa (ksi)]	21 (3,045)	5.1(739.6)/2.4 (348)	11.3 (16389)/3.1 (449.6)
Ultimate strain (%)	1.1±0.05	7.7±0.01	5.7±0.01

3.3. CONCRETE

The CFFT specimens were poured in one batch using the concrete mixture shown in Table 3. The average 28-day compressive strength of three concrete cylinders was determined per ASTM C39 as 48.3 MPa (7.0 ksi) with a standard deviation of 0.27.

Table 3: Concrete Mix

w/c	Cement [kg/m^3 (lb/ft^3)]	Water [kg/m^3 (lb/ft^3)]	Fine aggregate [kg/m^3 (lb/ft^3)]	Coarse aggregate [kg/m^3 (lb/ft^3)]
0.5	451 (28.15)	226 (14.1)	512 (32)	512(32)

4. TEST SETUP AND INSTRUMENTATION

The CFFT specimens were tested at ages ranging from 28 to 58 days. The CFFT specimens were tested using a MTS 2500 having a capacity of 2,400 kN (539 kips). At the beginning of testing a CFFT specimen, the MTS 2500 was preloaded with 44.5 kN (10.1 kips) to ensure full contact between the test specimen and the loading plate. The hoop and axial strains of the cylinders were measured using eight strain gauges located at the mid-height of each CFFT specimen (Fig. 5). Four push pots and two LVDTs that were 180^o apart were also installed to measure the axial displacements along the middle one-third and of the total heights, respectively, of each CFFT (Figs. 5 and 6). A data logger recorded the measured data.

The load was applied in a displacement control with a constant loading rate of 0.5 mm/minute (0.02 inch/minute). The cylinders were subjected to cyclic axial compression

loading until rupture of the FRP or reaching the ultimate load of the testing machine (Fig. 7). The loading steps included the following axial displacement of 0.02”, 0.04”, 0.08”, 0.12”, 0.16”, 0.20”, 0.35”, 0.50”, 0.75”, and 1.00” until failure. Each loading step was repeated for three cycles (Carter et al. 2014). During experiment, fixed-pinned testing condition was there; the top platen was fixed, and the bottom was a ball-jointed platen allowing free rotation to represent a pinned connection.

5. RESULTS AND DISCUSSION

5.1. GENERAL BEHAVIOR

Table 4 summarizes the results of the investigated CFFTs in terms of ultimate load capacity P_{max}, displacement, ultimate axial strain (ε_{lu}), and ultimate hoop strain (ε_{hu}). The axial strains were the average of the two LVDTs mounted on each specimen, while the hoop strains were the average value recorded by strain gauges mounted on each FRP tube.

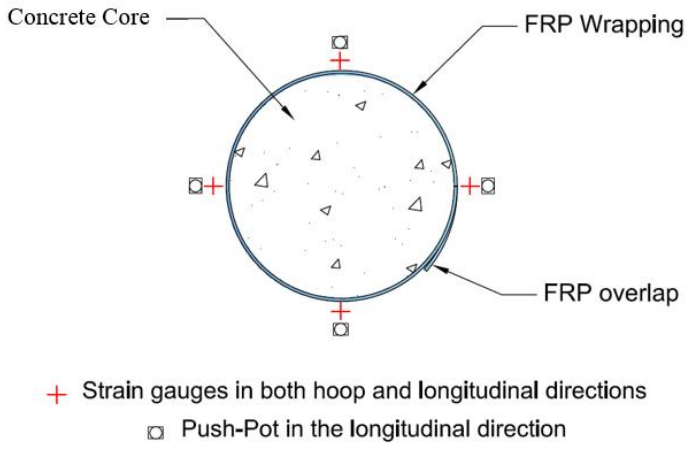

Fig. 5: Positions of strain gauges

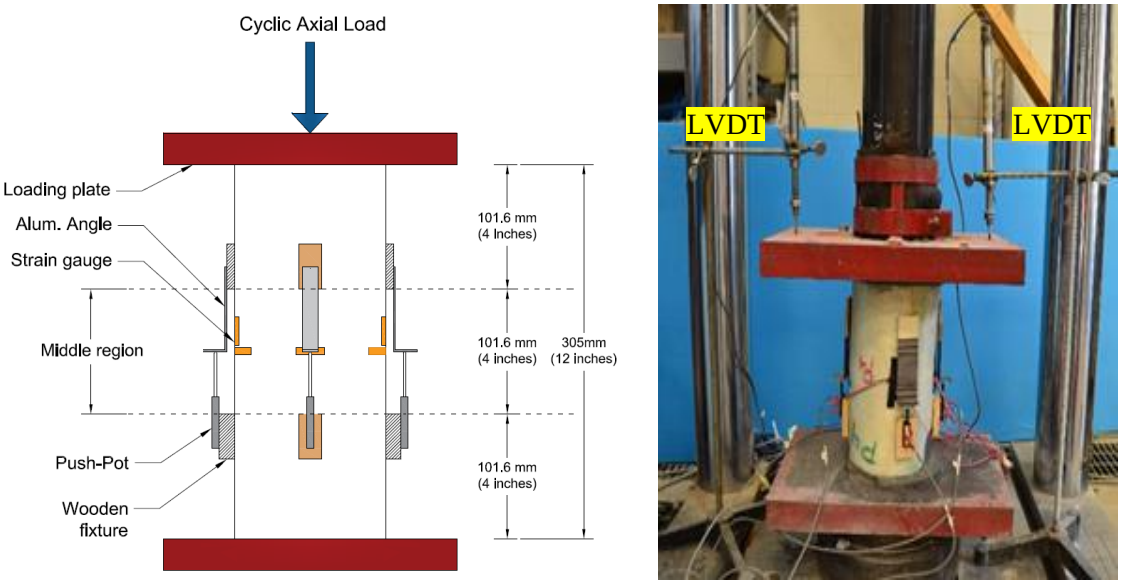

(a) (b)

Fig. 6: The CFFT (a) Instrumentation layout, and (b) Specimen during the test

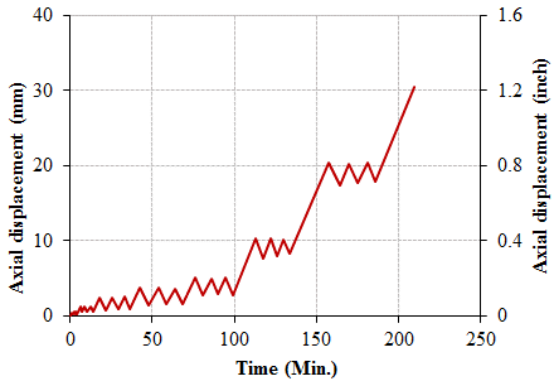

Fig. 7: Cyclic compression loading regime

As shown in table 4, LRS-CFFT specimens performed better than SRS-CFFT in terms of strength. H-CFFT outperformed the performance of LRS-PET-CFFT and SRS-CFFT. It is worth noting that the capacity of specimens P6, P10, and P12 exceeded the capacity of the MTS compression machine, so the specimens did not reach to their ultimate loads.

5.2. MODES OF FAILURE

Figs. 8 through 10 show the failure modes of the test specimens. Failure in all specimens occurred due to FRP rupture with loud noise in the case of SRS-FRP and limited noise in the case of LRS-FRP. Furthermore, the LRS-FRP rupture occurred locally along few horizontal circumferential lines typically at the mid-height of a test specimen as well as along few vertical lines (Figs. 8 and 9). The SRS-FRP rupture occurred along diagonal and zigzag lines with larger ruptured areas (Fig. 10) which explains the noise difference between rupture of LRS-FRP and SRS-FRP. Partial debonding of the FRP also occurred within the overlapping zone for few LRS-CFFT specimens; however, the final failure mode was due to FRP rupture.

Figs. 11 through 14 show the failure modes of the H-CFFT. The sequence of wrapping the FRP layers played an important role in determining the failure mode of the tested specimens. When the LRS-FRP layers were wrapped first (inside) followed by the SRS-FRP (outside), the failure dominated by rupture of the LRS-FRP. However, when the GFRP was inside and LRS-FRP was outside, failure was dominated by overlapping layer slippage and debonding. The reason might be bending of overlying layers caused by thicker LRS-FRP. In this case, the rupture of FRP is governed by GFRP (inside).

Table 4: Results of the tested Concrete-filled FRP Tubes

	Cylinder Label	FRP type	P_{max} [kN (kip)]	Ultimate Displacement [mm (inch)]	Ultimate Axial Strain (ε_{lu}) (%)	Ultimate Hoop Strain (ε_{hu}) %
LRS-CFFT	P1	PET	1,227 (276)	26.4 (1.04)	8.6	2.2
	P2		1,649 (371)	32.9 (1.3)	11.1	2.3
	P3		2,369 (533)	38.4 (1.5)	12.6	2.8
	P4	PEN	1,409 (317)	15.5 (0.6)	5.1	1.05
	P5		2,072 (466)	16.1 (0.6)	5.3	1.10
	P6		2,384 (536)*	19.4 (0.76)*	6.3*	0.85*
SRS-CFFT	P7	GFRP	1,372 (308)	5.9 (0.23)	1.9	0.44
	P8		1,822 (410)	9.2 (0.4)	2.9	0.54
	P9		2,035 (458)	8.3 (0.3)	2.7	0.55
H-CFFT	P10	PET-GFRP (in/out)	2,384 (536)*	17.6 (0.7)*	5.7*	1.38*
	P11		2,009 (452)	16.4 (0.65)	5.4	0.79
	P12	PEN-GFRP (in/out)	2,384 (536)*	36 (1.4)*	11.8*	1.2*
	P13		2,013 (453)	14 (0.6)	4.6	1.1
	P14	PET-GFRP (out/in)	1,895 (426)	18.2 (0.7)	5.9	0.67
	P15		2,012 (452)	25.1 (1)	8.2	2.1
	P16	PEN-GFRP (out/in)	2,133 (479)	12.9 (0.5)	4.2	0.76
	P17		2,100 (472)	24.3 (0.96)	7.9	N/A

* *The ultimate axial strength exceeded that of the MTS machine and*
* *N/A: malfunction strain gauges*

(a) (b) (c)

Fig. 8: PET-CFFTs rupture (a) P1 (1 layer), (b) P2 (2 layer), and (c) P3 (3 layer)

(a) (b) (c)

Fig. 9: PEN-CFFTs rupture (a) P4 (1 layer), (b) P5 (2 layer), and (c) P6 (3 layer)

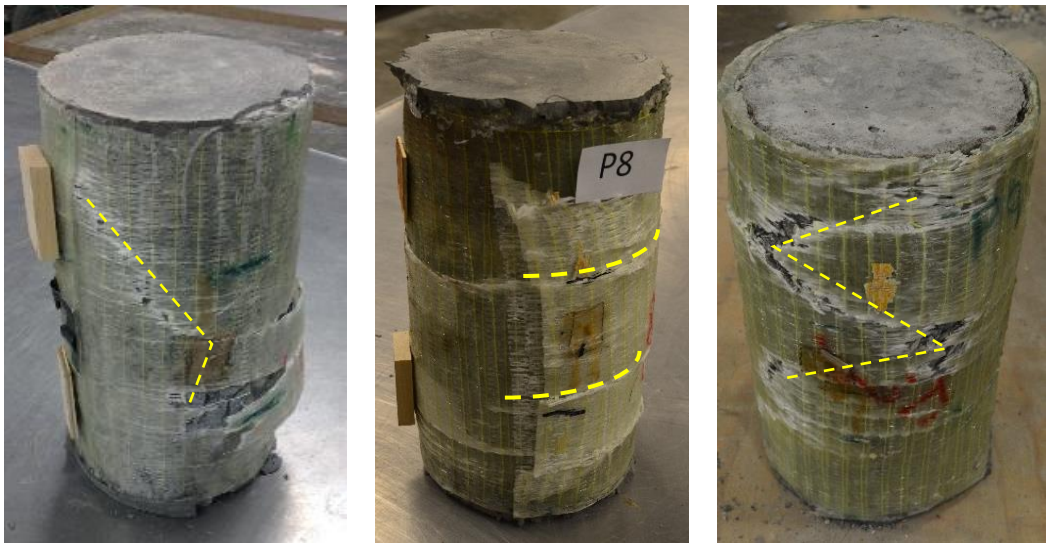

(a) (b) (c)

Fig. 10: GFRP-CFFTs rupture (a) P7 (1 layer), (b) P8 (2 layer), and (c) P9 (3 layer)

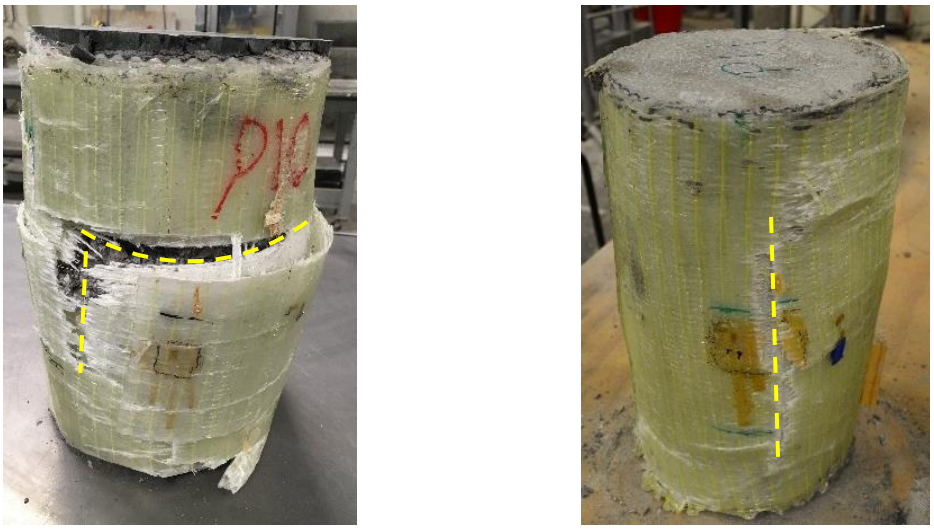

(a) (b)

Fig. 11: H-CFFT [in/out] rupture (a) P10 (2 PET/1 GFRP), and (b) P11 (1 PET/2 GFRP)

(a) (b)

Fig. 12: H-CFFT [in/out] rupture (a) P12 (2 PEN/1 GFRP), and (b) P13 (1 PEN/2 GFRP)

(a) (b)

Fig. 13: H-CFFT [in/out] rupture (a) P14 (1 GFRP/2 PET), and (b) P15 (2 GFRP/1 PET)

(a)

(b)

Fig. 14: H-CFFT [in/out] rupture (a) P16 (1 GFRP/2 PEN), and (b) P17 (2 GFRP/1 PEN)

5.3. STRESS-STRAIN BEHAVIOR

Figs. 15 through 21 represent the normalized stress (*f'cc/f'cu*) versus strain curves of the CFFTs'; where *f'cc* is the axial concrete confined stress and f'_{cu} is the axial stress of unconfined concrete. The horizontal positive axis represents axial strain; while the horizontal negative axis represents hoop strain.

For the PET-CFFTs (Fig. 15), the first portion of the normalized stress-strain curve was ascending parabolic-type, showing the increase in confined strength capacity by 1.4-2.7 as compared to unconfined concrete strength depending on the number of PET-FRP layers used. Beyond that a descending curve with the strength dropped to that of the unconfined concrete at axial strain of 2% was observed in both P1 and P2 (Figs. 15 (a) and (b)). However, using three layers of PET (Fig. 15 (c)), the strength loss in the second portion is insignificant and it can be considered as ascending curve. The reason is sufficient confinement provided by the three layers of PET-FRP. It is worth to mention that the reason

behind the second descending part drop was due to the lateral expansion of concrete, which leads to release of stress and drop was observed.

For the PEN-CFFTs, the first portion of the curve shows similar behavior as LRS-PET FRP with an increase in stress capacity by 1.5-2.5 over the unconfined concrete strength. The second part shows a small drop of strength and then followed by ascending curve. It is worth to mention that in Fig. 16 (c) (P6), the plateau at the top occurs because the MTS machine loading cell reached its capacity without rupture of the CFFT specimen.

In general, for the LRS-FRP, the descending curve for PET is followed by ascending curve, where passive confinement of FRP plays its main role, PET-FRP significantly recovers the strength loss and ductility is improved. While using the PEN-FRP significantly improves the strength and ductility of CFFTs'.

Fig. 17 shows the normalized stress-strain behavior of SRS-FRP tubes (P7, P8, and P9). The SRS-CFFTs' shows increase in capacity by 1.5-2.0 times the unconfined concrete strength with the increasing of the number of FRP layers used. However, small rupture strain value of 0.01%-0.025% was attained. The curve is ascending linearly up to ultimate strength until rupture with less ductility achieved.

For LRS-CFFT and SRS-CFFT, the ultimate strains for LRS-FRP are higher than the SRS-FRP for the same number of layer, and thereby LRS-CFFTs' provide better ductility than SRS-CFFTs'.

Figs. 18 to 21 show the normalized stress-strain behavior of H-CFFTs' (P10 to P17). The H-CFFTs' show almost the same behavior as of LRS, but the curve after strength drop i.e. initial rupture of FRP is either ascending or descending depending on the number of LRS FRP (PET or PEN) used.

For CFFTs' P10 (2 PET/1 GFRP) and P12 (2 PEN/1 GFRP) (Figs. 18 (a) and 19 (a)), before the strength drop there was an increase in the confined strength by 2.75 up to the axial strain of 3.5% and 5% for P10 and P12; respectively. After FRP rupture, the curve is ascending and able to recover 65% and 40% of the strength for P10 and P12; respectively, and provides ductility improvement observed noticeably for P12. For the specimens P11 (1 PET/2 GFRP) and P13 (1 PEN/2 GFRP) (Figs. 18 (b) and 19 (b)), the rupture axial strain was 2% and 1.5%; respectively, followed by descending curve with a negligible increase in strength.

For CFFTs' P14 (2 GFRP/1 PET) and P16 (2 GFRP/1 PEN) (Figs. 20 (a) and 21 (a)), the rupture axial strain was 2.3% and 3%; respectively, followed by a sharp descending curve with no increase in strength. For CFFTs' P15 (1 GFRP/2 PET) and P17 (1 GFRP/2 PEN) (Figs. 20 (b) and 21 (b)), there was an increase in the confined strength by 2.3 up to the axial strain of 2.3% and 2.8% for P15 and P17; respectively. After FRP rupture, the curve is ascending and able to recover 80% and 90% of the strength for P15 and P17; respectively, and provides more ductile behavior. It is worth to notice that in Fig. 21 (b), the only axial strain is shown due to some technical test deficiencies that prohibited the getting of the hoop strain values.

A hybrid system having 2 LRS FRP/1 GFRP reveals more strength gain and ductility improvement due to the sufficient confinement provided by LRS FRP. Moreover, in term of the H-CFFTs' strength, by placing LRS-FRP inside more confined strength has been attained reaching 2.75 for P10 and P12. However, in term of the H-CFFTs' ductility, by placing LRS-FRP outside more ductility behavior has been achieved.

To conclude, it is observed that in CFFTs' the first part of the curve is governed by the concrete strength and the slope is similar to both confined and unconfined concrete, whereas the second part is governed by characteristics of FRP and the slope increases by increasing number of layers. With the strength gain, ductility is also provided by LRS FRP in both LRS-CFFTs' and H-CFFTs' because of large rupture strain and efficient confinement.

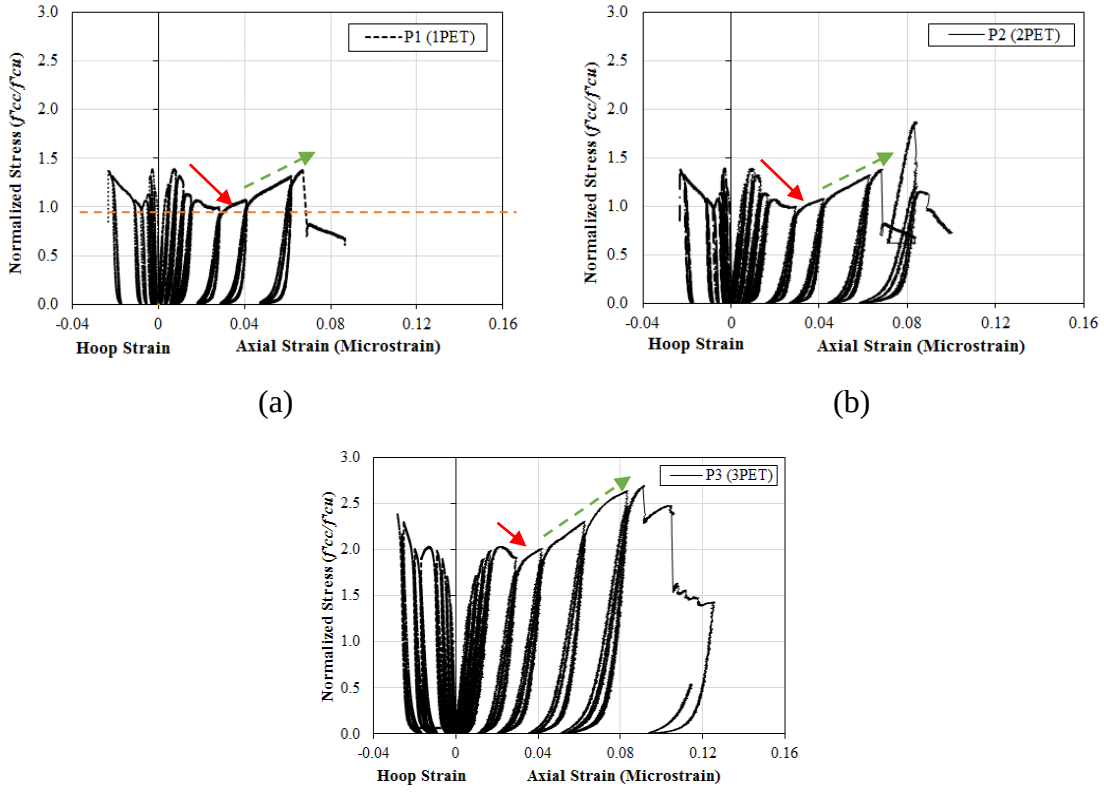

Fig. 15: Normalized stress via strain curves of PET-CFFTs (a) P1 (1 layer), (b) P2 (2 layers), and (c) P3 (3 layers)

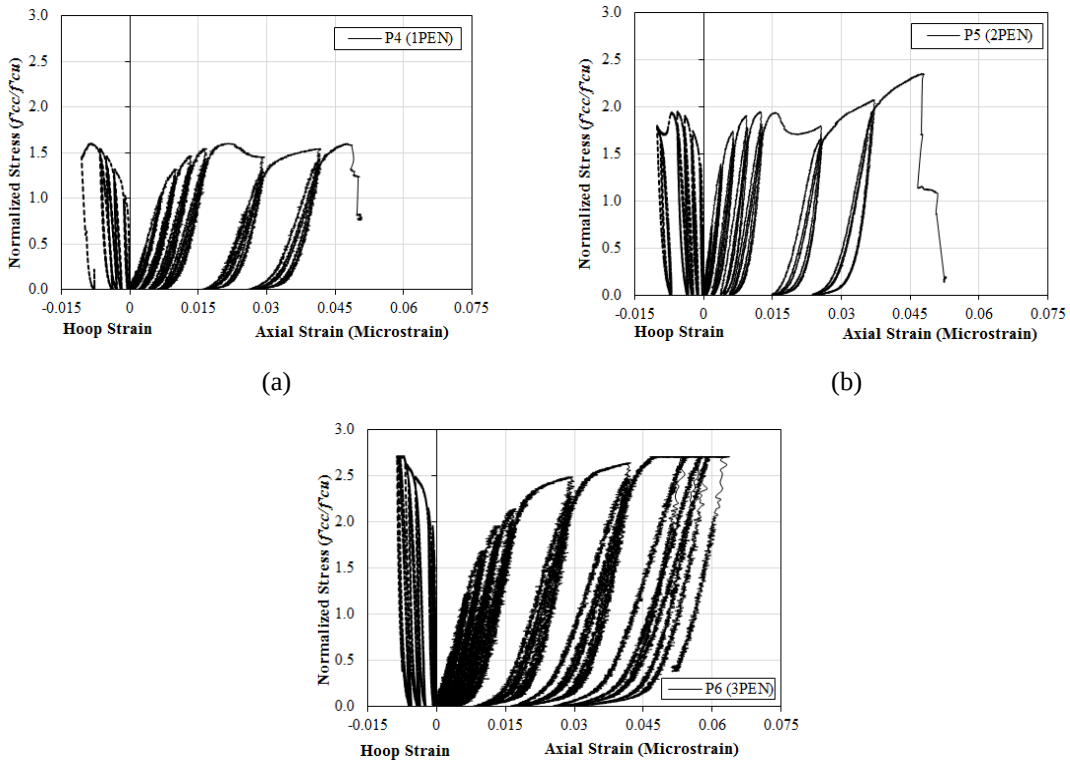

Fig. 16: Normalized stress via strain curves of PEN-CFFTs (a) P4 (1 layer), (b) P5 (2 layers), and (c) P6 (3 layers)

5.4. EFFECT OF CONFINEMENT PRESSURE

The ultimate capacity and stress-strain behavior of CFFTs are a function in the FRP confinement pressure. The stress-strain response of both FRP confined and unconfined concrete is similar when the applied axial stress is lower than the strength of unconfined concrete. However, when the axial stress reaches the maximum strength of unconfined concrete; then FRP starts applying pressure on the concrete core to counter the concrete dilation until the rupture of FRP. This lateral confinement provided by FRP to prevent the lateral expansion of concrete is passive in nature.

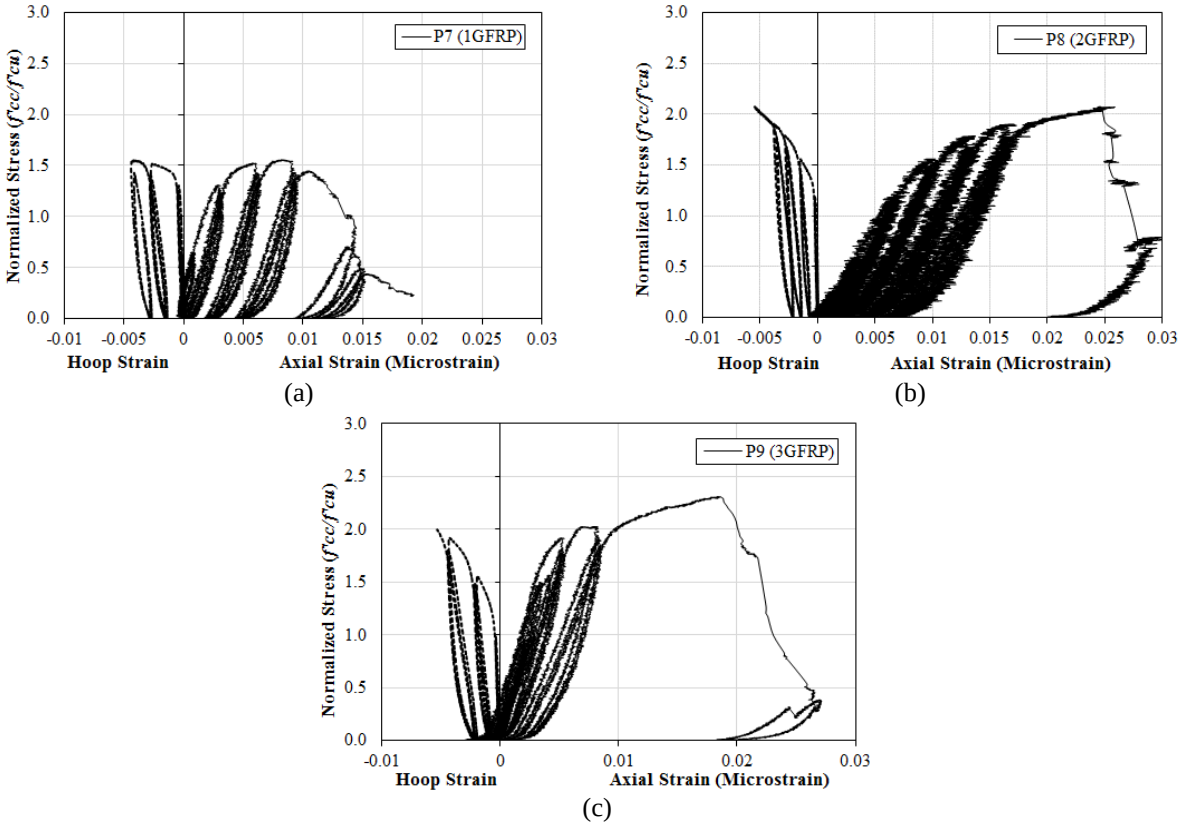

Fig. 17: Normalized stress via strain curves of GFRP-CFFTs (a) P7 (1 layer), (b) P8 (2 layers), and (c) P9 (3 layers)

The tension applied by the passive confinement of FRP in the hoop direction which prevents concrete failure and significantly improve the compressive strength and ductility of CFFTs. Therefore, the lateral confinement provided by FRP provides a highly ductile compression member despite the presence of brittle nature of both concrete and FRP. Table 5 shows the test results in terms of ultimate confinement effectiveness (*f'cc/f'c*) and strain gain with respect to confinement ratio (CR), where f'_{cc} is the ultimate strength of confined concrete, f'_c is the compressive strength of unconfined concrete i.e. 48.3 MPa (7 ksi), ε_{cc} and ε_{cu} (0.13 inch/inch) are the ultimate axial strain of the confined and unconfined concrete

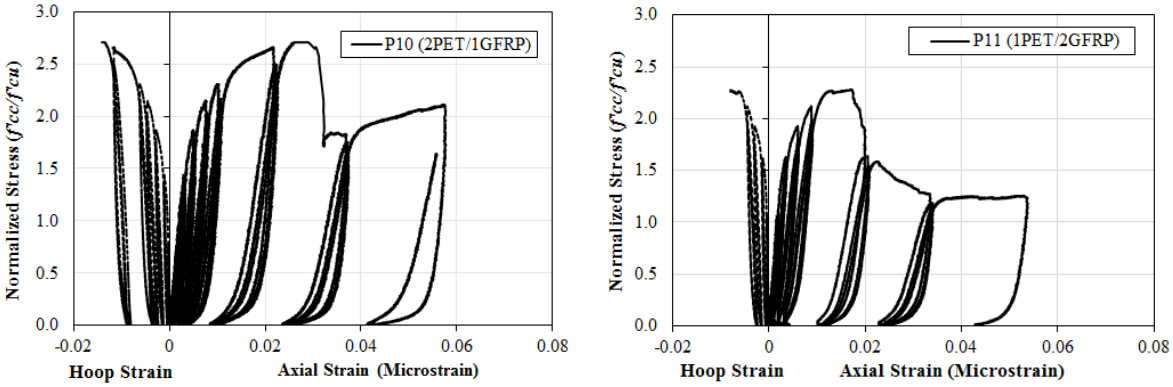

(a) (b)

Fig. 18: Normalized stress via strain curves of H-CFFTs (a) P10 (2 PET/1 GFRP), and (b) P11 (1 PET/2 GFRP)

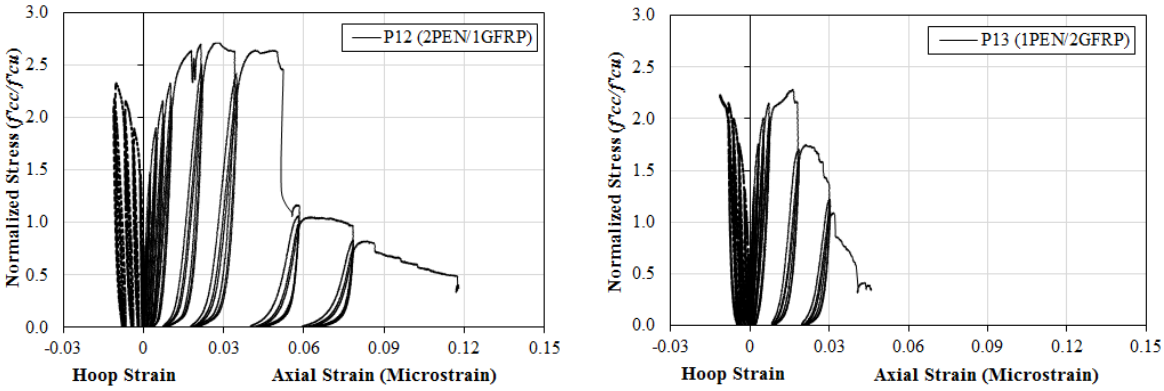

(a) (b)

Fig. 19: Normalized stress via strain curves of H-CFFTs (a) P12 (2 PEN/1 GFRP), and (b) P13 (1 PEN/2 GFRP)

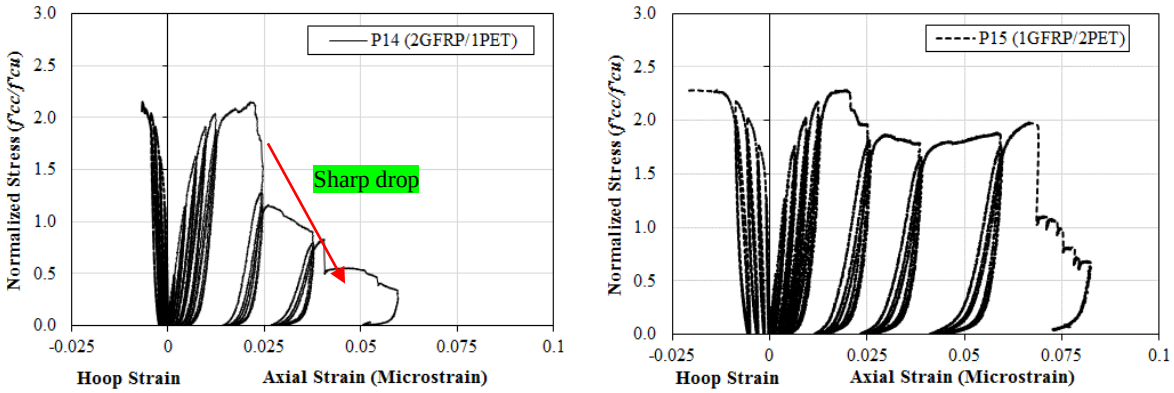

(a) (b)

Fig. 20: Normalized stress via strain curves of H-CFFTs (a) P14 (2 GFRP/1 PET), and (b) P15 (1 GFRP/2 PET)

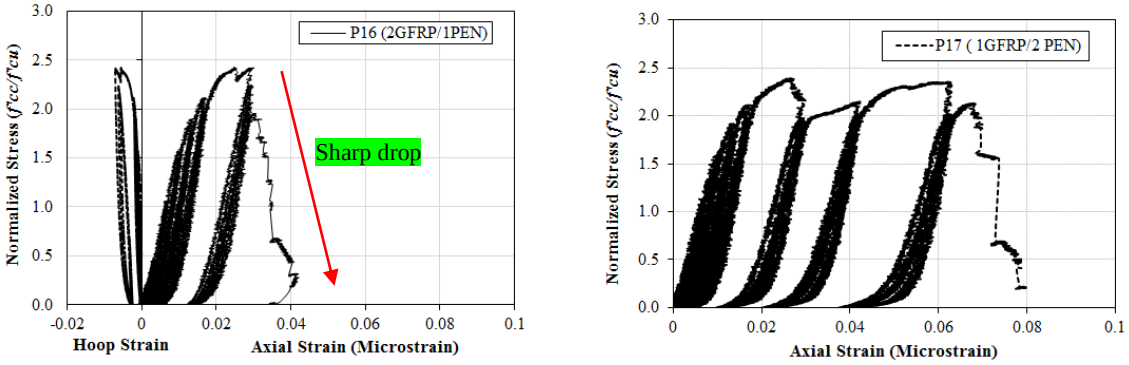

(a) (b)

Fig. 21: Normalized stress via strain curves of H-CFFTs (a) P16 (2 GFRP/1 PEN), and (b) P17 (1 GFRP/2 PEN)

respectively. Confinement efficiency increased with the CR increasing (Fig. 22). Despite having the same confinement ratio, LRS-CFFTs were more efficient than SRS-CFFTs in terms of providing an increase in load carrying capacity in the post-peak state (Fig. 22 (a)). The reason for this difference in the behavior can be the greater ultimate rupture strain value of LRS-FRP (greater than 5%) than glass FRP (2%). This clearly indicates the effect of higher rupture strain on the confinement which highly influences the behavior of concrete in terms of strength.

In case of LRS-CFFTs, both ductility and strength have increased with the increase in confinement ratio whereas the only strength of concrete improved for GFRP (Table 5). The ultimate axial strength of CFFTs' with PET and PEN was almost the same whereas, PET-CFFTs were more ductile than PEN-CFFTs. The reason was the higher value of ultimate strain and thickness in case of PET as compared to PEN-FRP. PET has reached the rupture strain value of up to 10%, PEN up to 6% whereas GFRP has lower rupture strain value of 2%.

In case of H-CFFTs, Fig. 22 (b) clearly indicate that the CFFTs having the sequence LRS-FRP inside and GFRP outside shows greater confinement effectiveness than GFRP inside and LRS-FRP outside sequence. The reason was confinement effectiveness in case of H-CFFT depends on the FRP present inside. Therefore, when LRS-FRP was inside it was more effective due to large rupture strain value than GFRP. It can also be observed that LRS-CFFTs having smaller CR than H-CFFTs have equal confinement effectiveness as of H-CFFT.

Table 5: Test Results of tested CFFTs

	f'_{cc} [MPa(ksi)]	Confinement effectiveness (f'_{cc}/f'_c)	ε_{cc} (inch/inch)	$\varepsilon_{cc}/\varepsilon_{cu}$	f_l^{**} [MPa (ksi)]	CR^{***}
P1	67.5 (9.78)	1.39	0.09	6.92	7.1 (1.02)	0.15
P2	90.3 (13.11)	1.87	0.11	8.46	14.2 (2.05)	0.29
P3	129.8 (18.84)	2.69	0.13	10.00	21.3 (3.08)	0.44
P4	77.2 (11.20)	1.60	0.05	3.85	9.1 (1.31)	0.19
P5	113.5 (16.47)	2.35	0.05	3.85	18.01 (2.6)	0.37
P6	130.5* (18.94)	2.71	0.06	4.62	27.1 (3.92)	0.56
P7	75.2 (10.91)	1.56	0.019	1.46	9.4 (1.36)	0.19
P8	99.9 (14.49)	2.07	0.03	2.31	18.7 (2.71)	0.39
P9	111.5 (16.18)	2.31	0.027	2.08	28.1 (4.07)	0.58
P10	130.7* (18.96)	2.71	0.057	4.38	23.5 (3.41)	0.49
P11	110.2 (15.98)	2.28	0.054	4.15	25.8 (3.74)	0.53
P12	130.6* (18.95)	2.71	0.118	9.08	27.4 (3.97)	0.57
P13	110.4 (16.01)	2.29	0.046	3.54	27.7 (4.02)	0.57
P14	103.8 (15.06)	2.15	0.059	4.54	25.8 (3.74)	0.53
P15	110.3 (16)	2.29	0.082	6.31	23.5 (3.41)	0.49
P16	116.9 (16.96)	2.42	0.04	3.08	27.7 (4.02)	0.57
P17	115.1 (16.7)	2.39	0.079	6.08	27.4 (3.97)	0.57

* *MTS machine capacity was reached*
** *Confinement pressure from Eq.2*
****CR: Confinement ratio from Eq.1*

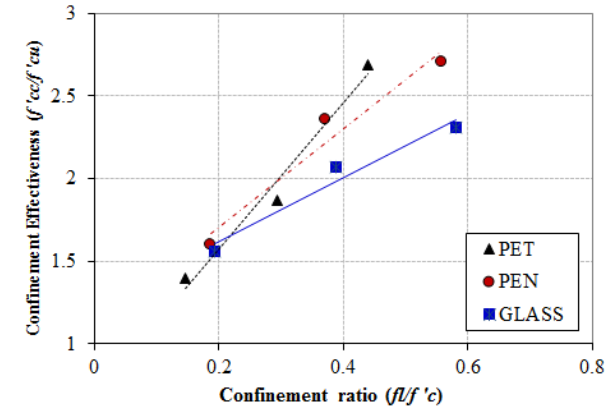

(a)

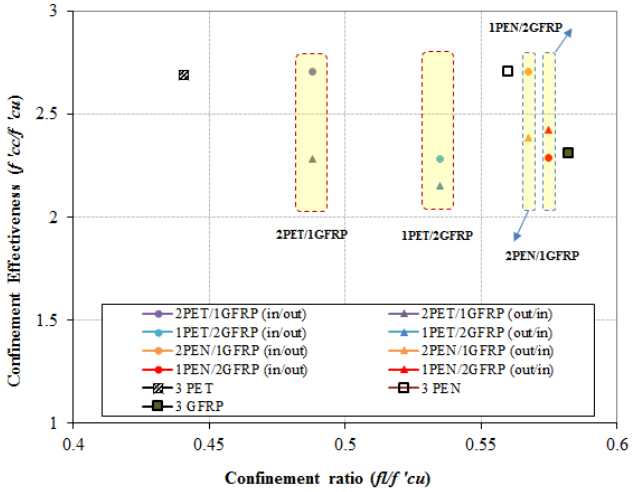

(b)

Fig. 22: Confinement effectiveness vs. confinement ratio of (a) LRS-CFFTs' and SRS-CFFTs' (P1-P9) (b) all 3 layers CFFTs'

5.5. EFFECT OF SEQUENCE OF HYBRID CFFTS

H-CFFTs' is investigated with different FRP application sequences by placing SRS-FRP at the inner surface (in)- in direct contact with the concrete infill; and LRS-FRP at the outer (out) surface in contact with the other FRP layer; and vice versa. From Fig. 23, it can be observed that there is 27% increase in stress and 50% in strain when LRS-FRP is placed inside and SRS-FRP outside. The reason for this was the difference between rupture

strain values of both FRP plies. When LRS-FRP was placed inside, the outer SRS-FRP was controlled by LRS-FRP and rupture occurred at higher hoop strain. However, when SRS-FRP was placed inside, the outer LRS-FRP was controlled by SRS-FRP and rupture occurred at lower hoop strain. In terms of strength and ductility, placing LRS-FRP inside and SRS-FRP outside improved the performance of such CFFT (Fig. 23).

In terms of energy dissipation, H-CCFTs' having LRS-FRP inside and SRS-FRP outside is an efficient system (Fig. 32) because of the effective confinement provided by PET and PEN to CFFT. Hence, H-CFFT having sequence LRS-FRP (inside) and SRS-FRP (outside) performs more efficient in terms of strength, ductility, and energy dissipation capacity.

5.6. DILATION PROPERTIES

To understand the behavior of CFFTs', it is important to study the volumetric response of concrete. The volumetric strain is defined as the volume change per unit volume change.

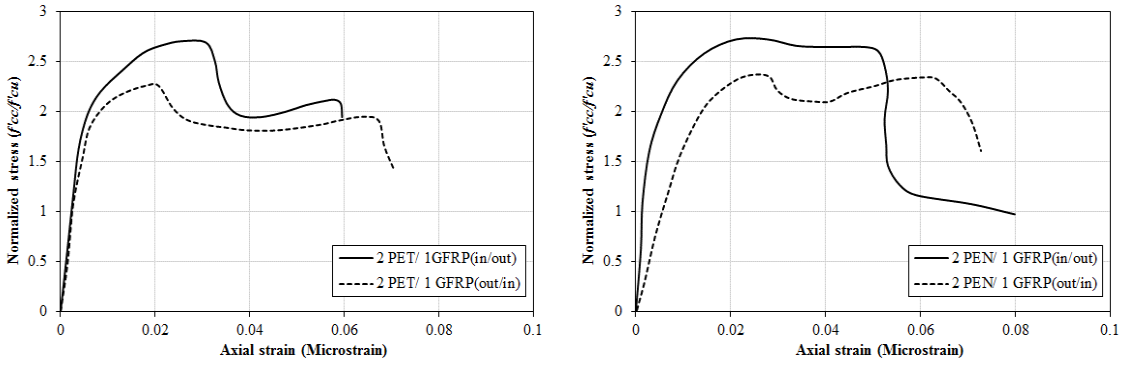

Fig. 23: Envelope curve for normalized stress via axial strain (a) 2 PET-1G-CFFT, and (b) 2 PEN-G-CFFT

$$\varepsilon_v = \varepsilon_l + 2\varepsilon_r \quad (3)$$

where ε_v is volumetric strain, ε_l is an axial strain, and ε_r is hoop strain. It is well known that unconfined concrete experiences a volume reduction up to 0.9 *f'c*, thereafter concrete experiences volume expansion i.e. volume change direction is reversed. This volume expansion is unstable beyond the peak strength. However, it is observed that in case of CFFTs', the linearly increasing hoop stress eventually reduce this volume expansion if an adequate amount of confinement by FRP is provided (Samaan et al. 1998).

Figs. 24 to 26 shows the volumetric strain curves for CFFTs'. Volume reduction and volume expansion are shown on positive and negative axis, respectively. For one and two layers of PET-CFFTs (Fig. 24(a)), it can be observed that direction of volumetric strain changes from reduction to expansion below the compressive strength of concrete once but expansion is soon taken over by reduction. Hence, concrete failed in compaction. However, for three layers of PET compaction is taken over by expansion at a normalized axial stress of approximately 1.8, but in the end, concrete failed in compaction (Fig. 24 (a)).

From Figs. 24 (b), despite some volume expansion beyond the compressive strength of concrete, volume expansion is curtailed by increasing hoop stress of FRP. For three layers of PEN-CFFTs (Fig. 24 (b)), it can be observed that volumetric strain changes from reduction to expansion at the normalized axial stress of 2, and this expansion continues to increase until rupture.

From Fig. 24 (c), it can be observed that volume expansion continues until failure after initial volume reduction of concrete up to the compressive strength of concrete. This is due to inadequate confinement provided by SRS-CFFTs'. For PET-G-CFFTs', it is observed that volumetric strain changes from reduction to expansion above the

compressive strength of unconfined concrete at 1.5 (Fig. 25). This expansion continues until failure. For 2-PEN-1-G-CFFTs', similar behavior is observed as of PET-G-CFFTs' (Fig. 25). However, in case of 1-PEN-2-G-CFFTs' failure is due to volume expansion experienced at below compressive strength of compressive strength of unconfined concrete at 0.8 (Fig. 26).

For SRS-LRS-CFFTs (Figs. 25 and 26), it is observed that volumetric strain changes from reduction to expansion above the compressive strength of unconfined concrete at 1.5 and 2 respectively.

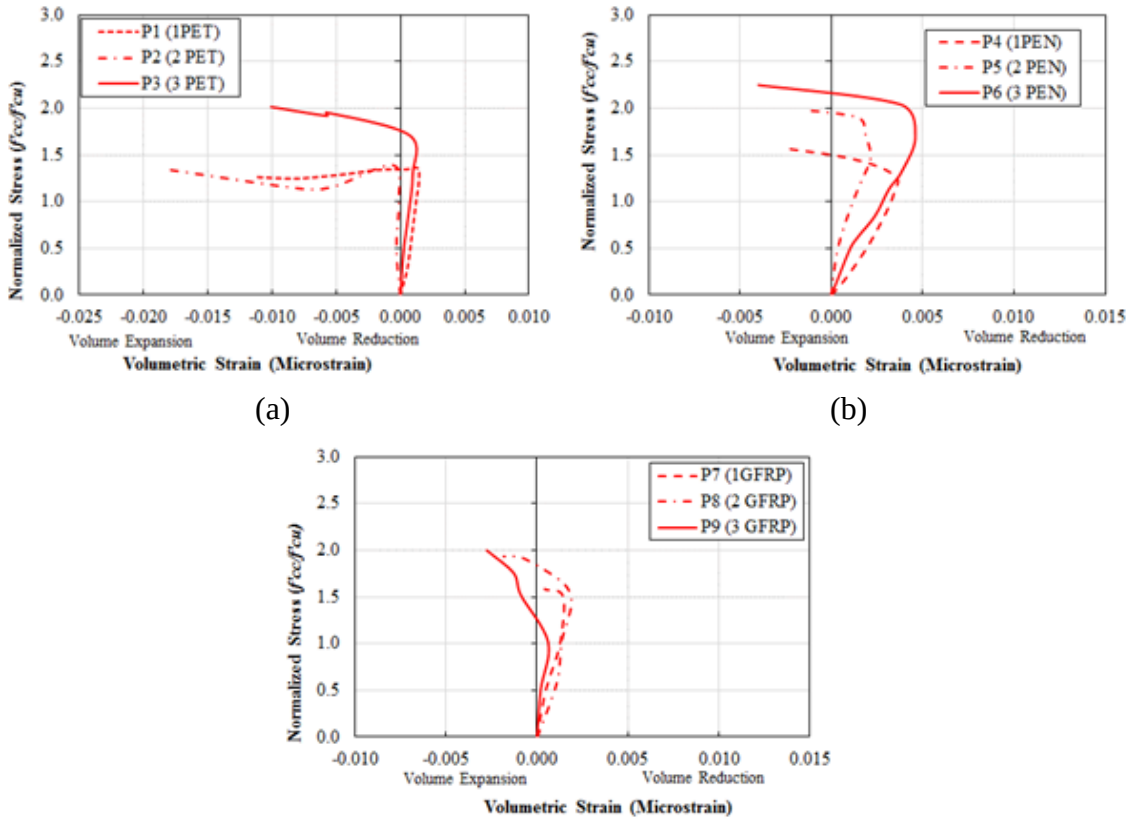

Fig. 24: Volumetric strain (ε_v) curves (a) PET-CFFTs, (b) PEN-CFFTs, and (c) SRS-CFFTs

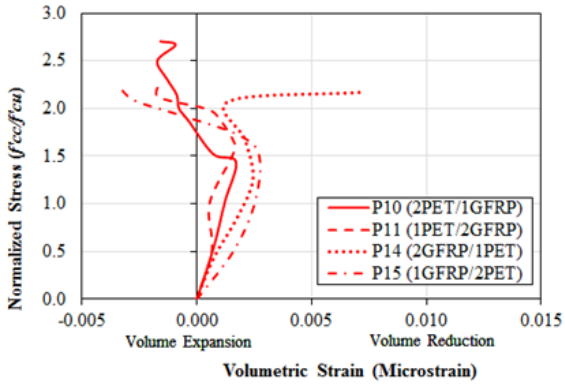

Fig. 25: Volumetric Strain curves of H-CFFTs

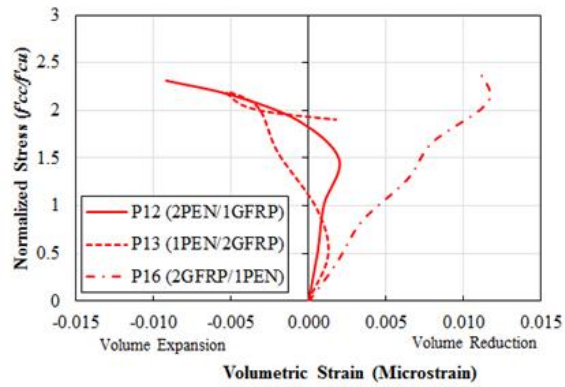

Fig. 26: Volumetric Strain curves of H-CFFTs

It can be concluded from the above discussion that the increasing hoop stress of FRP curtails the volume expansion and with an adequate amount of confinement from FRP volume expansion can be effectively prevented.

5.7. ENERGY DISSIPATION

Cumulative energy dissipation is a crucial parameter as it is a measure of the ability of a structural member to dissipate the input seismic and hence to sustain the earthquake ground motions. In cyclic load experiment, the dissipated energy can be calculated as the difference between the input energy; i.e. toughness, and elastic energy. Hence, the dissipated energy in any given cycle of loading can be calculated as the area enclosed by

the load-displacement curve. The cumulative energy dissipation is calculated by adding the values of energy dissipated for the first cycle of each loading displacement protocol. Figs. 27 to 29 show the relationship between the cumulative dissipated energy and the axial displacement for the CFFT specimens.

LRS-FRP have the lower stiffness value which can be a concern for the sudden failure of CFFTs'. However, from Figs. 27 (a) and (b), it can be concluded that energy dissipation capacity of LRS-CFFTs' is significant. The large rupture strain values of PET and PEN-FRP balances the lower stiffness of LRS-FRP, and prevent the sudden failure of CFFTs'. SRS-FRP having higher stiffness have a lower value of energy dissipated compared to LRS FRP (Fig. 28). PET has a 466.6% more energy dissipation capacity than SRS-FRP whereas PEN has 220% more energy dissipation capacity than SRS-FRP. It can be concluded that LRS-CFFTs' shows an efficient system to be used in seismic areas as energy dissipation capacity of LRS-FRP is significant.

From Fig. 29, it can be observed that PET-G-CFFTs' also exhibit a significant energy dissipation by 286.7% more than SRS-CFFTs' (Fig. 29 (a)), whereas PEN-G-CFFTs' has 506% more energy dissipation capacity than SRS-CFFTs' (Fig. 29 (b)).

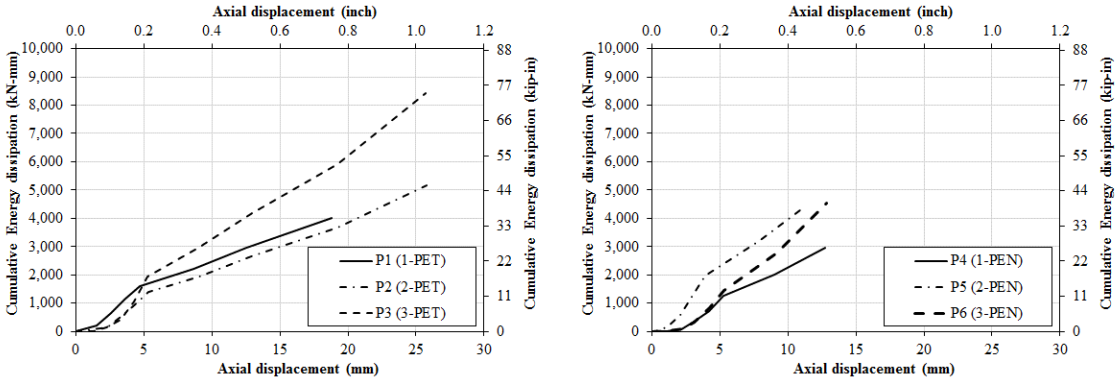

(a) (b)

Fig. 27: Cumulative energy dissipation via axial displacement of LRS-CFFTs (a) PET-CFFTs, and (b) PEN-CFFTs

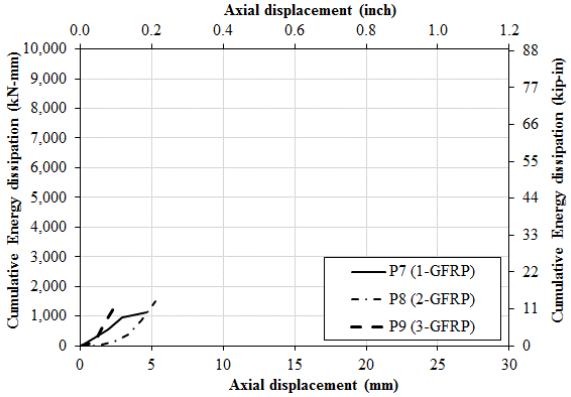

Fig. 28: Cumulative energy dissipation via axial displacement of SRS-CFFTs

.

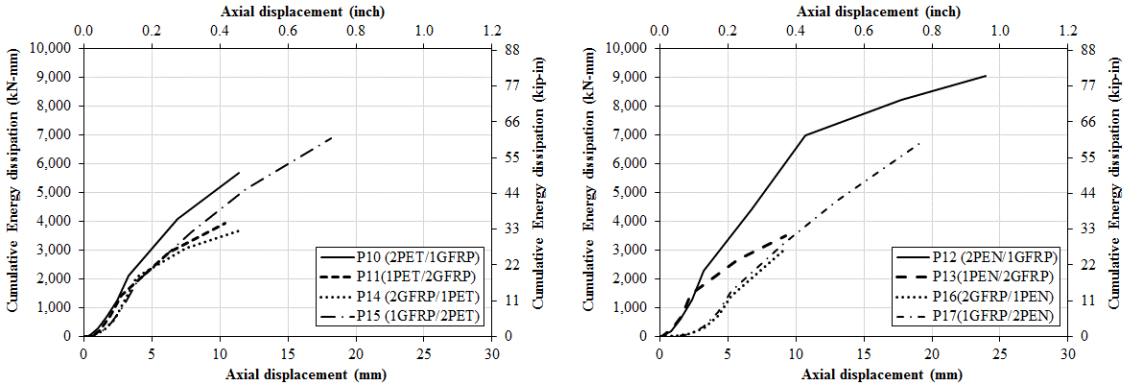

(a) (b)

Fig. 29: Cumulative energy dissipation via axial displacement of H-CFFTs (a) PET-G-CFFT, and (b) PEN-G-CFFT

5.8. ULTIMATE STRENGTH EVALUATION OF CFFTS USING EXISTING MODELS

The ultimate compressive strengths obtained from the experimental results are compared with confinement analytical models developed by Saafi et al. (1999), Shehata et al. (2002), Ilki and Kumbasar (2003), Shao et al. (2006), and Teng et al. (2009) as shown in Table 6. Fig. 30 shows the compressive strength values of the obtained test results of the 17 CFFTs' (Table 1) compared to the analytical models. While Table 7 shows the statistical analysis of the models accuracy by using three statistical indicators (Average, standard deviation (STD), and coefficient of variance (COV)).

Based on the general observation, it can be seen from Table 6 and Fig. 34 that the analytical models proposed by Teng et al. (2009) and Shao et al. (2006) were in close accuracy agreement with the obtained experimental results for lower confinement ratio values. However, for higher confinement ratio values, Teng et. al. (2009) overestimated

and Shao et. al. (2006) underestimated the strength. While the others existing models were underestimated the strength by 14%. No model present in the study was able to estimate the behavior for high confinement ratio values.

Table 6: Available analytical confinement models

Model	Confined Compressive Strength	Confinement pressure f_l	
(Saafi et al. 1999)	$\frac{f'_{cc}}{f'_{co}} = 1 + 2.2(\frac{f_l}{f'_{co}})^{-0.16}$	$f_l = \frac{2f_f nt_f}{D}$	(4)
(Shehata et al. 2002)	$\frac{f'_{cc}}{f'_{co}} = 1 + 2.0\frac{f_l}{f'_{co}}$	$f_l = \frac{2f_f nt_f}{D}$	(5)
(Ilki and Kumbasar 2003)	$\frac{f'_{cc}}{f'_{co}} = 1 + 2.23\frac{f_l}{f'_{co}}^{0.7}$	$f_l = \frac{f_f \rho_f}{2}$ $\rho_f = \frac{4nt_f}{D}$	(6)
(Shao et al. 2006)	$\frac{f'_{cc}}{f'_{co}} = 1 + 6\frac{f_l}{f'_{co}}$	$f_l = \frac{2f_f nt_f}{D}$	(7)
(Teng et al. 2009)	$\frac{f'_{cc}}{f'_{co}} = 1 + 3.5\frac{f_{le}}{f'_{co}}$	$f_{le} = \frac{\varepsilon_{fe} E_f nt_f}{R}$	(8)

Table 7: Statistical result of the evaluated analytical models

Model	Average	Standard Deviation	COV	# over estimated CFFTs'
Saafi et al. (1999)	1.14	0.12	0.11	5
Shehata et al. (2002)	0.95	0.09	0.09	0
Ilki and Kumbasar (2003)	0.85	0.08	0.09	1
Shao et al. (2006)	0.90	0.08	0.09	3
Teng et al. (2009)	0.93	0.09	0.10	14

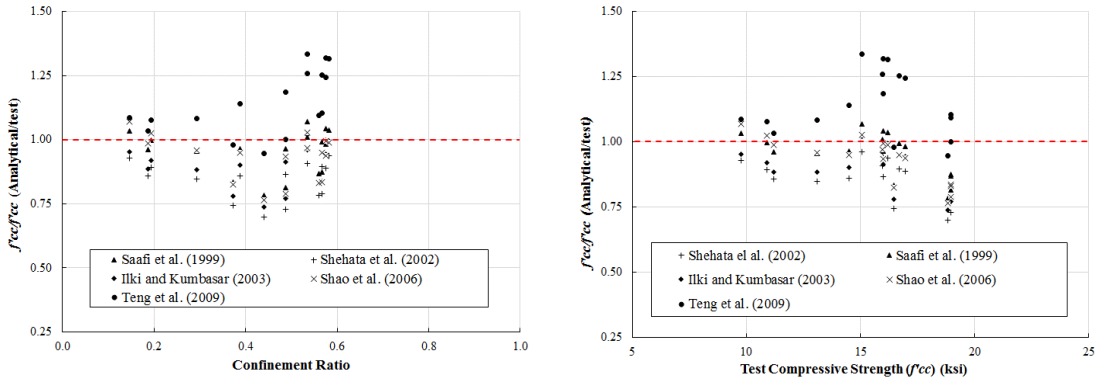

Fig. 30: Ratio of analytical compressive strength and test compressive strength via (a) confinement ratio, and (b) test compressive strength

6. CONCLUSION

In this paper, an experimental study was investigated to explain the cyclic compressive behavior of concrete confined to large rupture strain FRP (LRS-FRP) or hybrid LRS-FRP and G-FRP (SRS-FRP). Seventeen cylinders were tested for different confinement ratio.

1. LRS-FRP is more efficient in terms of strength and ultimate strain than SRS-FRP. LRS-FRP reached the ultimate rupture strain up to 10% whereas SRS-FRP's strain value is 2%.
2. In terms of strength gain, ductility, and energy dissipation capacity, PET-FRP has better performance than PEN-FRP.
3. Increasing the confinement by more number of layers of LRS-FRP leads to increase in strength and ultimate strain as similar to SRS-FRP.

4. In terms of strength, H-CFFTs' is more efficient than both the LRS-FRP and SRS-FRP. In terms of ultimate strain, H-CFFTs' showed higher ultimate strain than SRS-FRP and PEN but PET-FRP alone is more efficient.
5. In terms of wrapping sequence in H-CFFTs, H- CFFT having LRS-FRP inside and SRS-FRP outside was effective in terms of strength and increases ultimate axial strain.
6. LRS-CFFTs' and H-CFFTs' both are efficient in terms of energy dissipation.

Finally, the new H-CFFTs' is a promising system for improved durability and strength of concrete-filled FRP tubes. In seismic areas, it can be an effective system due to its ductility and energy dissipated capacity.

REFERENCES

Abdelkarim, O. I., and ElGawady, M. A. (2014). "Analytical and finite-element modeling of FRP-concrete-steel double-skin tubular columns." *Journal of Bridge Engineering*, 20(8), B4014005.

Abdelkarim, Omar I., and Mohamed A. ElGawady. "Concrete-filled-large deformable FRP tubular columns under axial compressive loading." *Fibers3*, no. 4 (2015): 432-449.

Abdelkarim, O. I., ElGawady, M. A., Gheni, A., Anumolu, S., and Abdulazeez, M. (2016). "Seismic Performance of Innovative Hollow-Core FRP–Concrete–Steel Bridge Columns." *Journal of Bridge Engineering*, 04016120.

Abdulazeez, M. M., and ElGawady, M. A. (2017). "Nonlinear Analysis of Hollow-Core Composite Building Columns." *Proc., SMAR 2017, ETH Zurich.*

Abdulazeez, M. M., Gheni, A., Abdelkarim, O. I., and ElGawady, M. A. (2017). "Seismic Behavior of Precast Hollow-Core FRP-Concrete-Steel Column having Socket Connection." *Proc., Transportation Research Board (TRB) 96th Annual Meeting*.

Anggawidjaja, D., Ueda, T., Dai, J., and Nakai, H. (2006). "Deformation capacity of RC piers wrapped by new fiber-reinforced polymer with large fracture strain." *Cement and Concrete Composites*, 28(10), 914-927.

Bai, Y.-L., Dai, J.-G., and Teng, J. (2013). "Cyclic compressive behavior of concrete confined with large rupture strain FRP composites." *Journal of Composites for Construction*, 18(1), 04013025.

Bai, Y. (2014). "Behavior and modeling of RC columns confined with large-rupture strain FRP composites." The Hong Kong Polytechnic University.

Carter, J., Abdelkarim, O., ElGawady, M., and Khayat, K. (2014) "FRP Confinement of High Strength Self-Consolidating Concrete." *Proc., 10th US National Conf. on Earthquake Engineering, Alaska, USA.*

Chen, W.-F. (2007). *Plasticity in reinforced concrete*, J. Ross Publishing.

Dai, J.-G., Bai, Y.-L., and Teng, J. (2011). "Behavior and modeling of concrete confined with FRP composites of large deformability." *Journal of Composites for Construction*.

Dai, J., and Bai, Y. (2014). "Large rupture strain (LRS) fibre-reinforced polymer (FRP) composites for seismic retrofit of reinforced concrete (RC) piers." Woodhead Publishing.

Fam, A., and Rizkalla, S. (2001). "Behavior of axially loaded concrete-filled circular FRP tubes." *A CI Structural J*, 98(3), 280-289.

Fam, A. Z., and Rizkalla, S. H. (2002). "Flexural behavior of concrete-filled fiber-reinforced polymer circular tubes." Journal of Composites for Construction, 6(2), 123-132.

Ilki, A., and Kumbasar, N. (2003). "Compressive behaviour of carbon fibre composite jacketed concrete with circular and non-circular cross-sections." Journal of Earthquake *Engineering*, 7(03), 381-406.

Jirawattanasomkul, T., Dai, J.-G., Zhang, D., Senda, M., and Ueda, T. (2013). "Experimental study on shear behavior of reinforced-concrete members fully wrapped with large rupture-strain FRP composites." Journal of Composites for Construction, 18(3), A4013009.

Lam, L., and Teng, J. (2001) "A new stress-strain model for FRP-confined concrete." *Proc., FRP Composites in Civil Engineering. Proceedings of the International Conference on FRP composites in Civil EngineeringHong Kong Institution of Engineers, Hong Kong Institution of Steel Construction.*

Mirmiran, A., and Shahawy, M. (1997). "Behavior of concrete columns confined by fiber composites." Journal of Structural Engineering, 123(5), 583-590.

Mirmiran, A., Shahawy, M., Samaan, M., Echary, H. E., Mastrapa, J. C., and Pico, O. (1998). "Effect of column parameters on FRP-confined concrete." Journal of Composites for Construction, 2(4), 175-185.

Moustafa, A., and ElGawady, M. A. (2016). "Strain rate effect on properties of rubberized concrete confined with glass fiber–reinforced polymers." Journal of Composites for Construction, 20(5), 04016014.

Ozbakkaloglu, T. (2013). "Compressive behavior of concrete-filled FRP tube columns: Assessment of critical column parameters." Engineering Structures, 51, 188-199.

Ozbakkaloglu, T., and Akin, E. (2011). "Behavior of FRP-confined normal-and high-strength concrete under cyclic axial compression." *Journal of Composites for Construction*, 16(4), 451-463.

Ozbakkaloglu, T., and Oehlers, D. J. (2008). "Concrete-filled square and rectangular FRP tubes under axial compression." Journal of Composites for Construction, 12(4), 469-477.

Rousakis, T. C. (2013). "Elastic fiber ropes of ultrahigh-extension capacity in strengthening of concrete through confinement." Journal of Materials in Civil Engineering, 26(1), 34-44.

Saafi, M., Toutanji, H. A., and Li, Z. (1999). "Behavior of concrete columns confined with fiber reinforced polymer tubes." ACI materials journal, 96(4), 500-509.

Saleem, S., Hussain, Q., and Pimanmas, A. (2016). "Compressive Behavior of PET FRP–Confined Circular, Square, and Rectangular Concrete Columns." *Journal of Composites for Construction*, 21(3), 04016097.

Samaan, M., Mirmiran, A., and Shahawy, M. (1998). "Model of concrete confined by fiber composites." Journal of structural engineering, 124(9), 1025-1031.

Shao, Y., Zhu, Z., and Mirmiran, A. (2006). "Cyclic modeling of FRP-confined concrete with improved ductility." Cement and Concrete Composites, 28(10), 959-968.

Shehata, I. A., Carneiro, L. A., and Shehata, L. C. (2002). "Strength of short concrete columns confined with CFRP sheets." *Materials and Structures*, 35(1), 50-58.

Teng, J., Jiang, T., Lam, L., and Luo, Y. (2009). "Refinement of a design-oriented stress–strain model for FRP-confined concrete." Journal of Composites for Construction, 13(4), 269-278.

Youssf, O., ElGawady, M. A., Mills, J. E., and Ma, X. (2014). "Finite element modelling and dilation of FRP-confined concrete columns." *Engineering Structures*, 79, 70-85.

II.BEHAVIOR OF CONCRETE-FILLED HYBRID SMALL AND LARGE RUPTURE STRAIN FRP TUBES UNDER CYCLIC AXIAL COMPRESSION

Monika Nain[4]; Mohanad M. Abdulazeez [5], S.M.ASCE; and Mohamed A. ElGawady[6§], Ph.D., M. ASCE

ABSTRACT

This paper presents the results of an experimental study on the behavior of concrete filled fiber reinforced polymer (FRP) tubes (CFFTs) under cyclic axial compression. The main objective of this study is to observe the compressive behavior of large rupture strain FRP (LRS-FRP), small rupture strain FRP (SRS-FRP) and hybrid LRS-SRS-FRP CFFTs. Twelve cylinders having different confinement ratios investigated to understand the behavior of CFFTs in terms of ductility, ultimate strain, confinement effectiveness, and energy dissipation capacity. Owing to the large rupture strain property of LRS-FRP, CFFTs shows highly ductile behavior and significant energy dissipation capacity. The hybrid CFFT improves the ductility and energy dissipation capacity of the SRS-FRP confined concrete.

[4]Graduate Research Assistance, Dept. of Civil, Architectural, and Environmental Engineering, Missouri University of Science and Technology, Rolla, MO. 65409; mnb94@mst.edu
[5]Graduate Research Assistance and PhD student, Dept. of Civil, Architectural, and Environmental Engineering, Missouri University of Science and Technology, Rolla, MO. 65409; mma548@mst.edu
[5] Benavides Associate Professor, Dept. of Civil, Architectural, and Environmental Engineering, Missouri University of Science and Technology, Rolla, MO. 65409; elgawadym@mst.edu
[§]Corresponding author

1. INTRODUCTION

External confinement of concrete with FRP has proven to be able to increase the strength and ductility of the structures. Application of FRP instead of steel is preferable due to easy installation, high strength to weight-ratio, corrosion resistance, and relatively low maintenance cost. FRP materials such as carbon, glass, and aramid are frequently used FRPs types in the market. Many researchers have proven their application in strength enhancement (Choi and Xiao 2009; Dawood and ElGawady 2013; Fanggi and Ozbakkaloglu 2013; Mirmiran and Shahawy 1997; Ozbakkaloglu et al. 2013; Seible et al. 1997; Shao 2003; Spoelstra and Monti 1999; Wu and Wei 2010). However, due to small rupture strain (SRS) their application is limited in seismic areas as the fiber ruptured sooner and does not provide ductility.

In recent years, a new category of FRP has emerged as an alternative to SRS-FRPs called LRS-FRP. LRS-FRP include PEN (polyethylene napthalate) and PET (polyethylene terephthalate) having properties of large rupture strain (LRS), larger than 5%, and low stiffness (Bai et al. 2013; Bai 2014; Dai and Ueda 2012; Nain et al. 2017; Saleem et al. 2018). Due to large rupture strain, they can fulfill the ductility requirement and strengthening in seismic areas. Moreover, LRS-FRP are usually made of recycled materials (plastic bottles) giving cheaper and environment friendly solution.

Despite the large number of studies on CFFTs, fewer studies are available on LRS-FRP as most of them are focused on SRS-FRP behavior (Anggawidjaja et al. 2006; Dai et al. 2011; Dai and Bai 2014). These studies showed that LRS-CFFTs can lead to more ductile behavior and energy dissipation capacity with same level of strength enhancement.

Most of research work presented studies on comparison between the behavior of SRS-CFFTs and LRS-CFFTs but Abdelkarim and ElGawady (2015) were the first to numerically investigate the performance of hybrid LRS-SRS-FRP (H-CFFT) confined concrete under monotonic axial compressive loading. No experimental work has been done to study the effect of this new H-CFFT with different combination of FRP under cyclic axial compression. The study showed the outstanding performance of H-CFFT in terms of ductility, deformation capacity, and energy dissipation capacity.

2. RESEARCH SIGNIFICANCE

Many experimental and analytical studies on the compressive behavior of SRS-CFFT have been carried out, comparatively less research work has been done on LRS-FRP. Moreover, most of the studies are exclusively focused on monotonic behavior. For the seismic design and retrofit of structural members, it is necessary to understand the behavior of CFFTS under cyclic axial compression. A very limited experimental work has been done on the cyclic compressive behavior (Bai et al. 2013; Bai 2014; Jirawattanasomkul et al. 2013; Rousakis 2013). This paper is therefore experimentally investigates the performance of LRS-CFFTs (PET AND PEN), SRS-CFFTs with carbon FRP (CFRP), and H-CFFTs under cyclic axial compressive loading.

The study reported in this paper was aimed at investigating the effects of the types of fiber (PET, PEN, and Carbon) on the behavior of CFFTs in terms of strength, ductility, and energy dissipation.

3. EXPERIMENTAL PROGRAM

In this study, twelve CFFTs having different confinement ratio (CR) were tested under cyclic axial compression (Table 1). The dimension of each cylinder was 156 mm x 305 mm (6 inch x 12 inch). The CR (Equation 1) is defined as the ratio of confining pressure (f_l) and compressive strength of unconfined concrete (f'_c).

$$CR = \frac{f_l}{f'_c} \tag{1}$$

$$f_l = {}^{2E_f \varepsilon_f t_f}\Big/_{D_f} \tag{2}$$

where E_f is the FRP tube hoop modulus of elasticity, t_f is the total thickness of the FRP tube, ε_f is the hoop ultimate tensile strain of the FRP tube, and D_f is the internal diameter of the FRP tube.

In this study, CFFTs were majorly divided into three categories (Table 1) depending on the type of FRP used (Fig. 1): LRS-CFFT, SRS-CFFT, and H-CFFT. LRS-CFFT stands for large rupture strain FRP i.e. PET and PEN having six cylinders (P1 to P6) with varying FRP layers ranging from one to three. SRS-CFFT stands for small rupture strain FRP i.e. carbon having three cylinders (C1 to C3) with varying FRP layers ranging from 1 to 3. H-CFFT stands for hybrid CFFT, using both LRS and SRS FRP. It consists of 3 cylinders (C4 to C6) having LRS-FRP inside and SRS-FRP outside. From previous studies (Nain et al. 2017), it is observed that in case of H-CFFTs sequence of LRS-SRS (in/out) was more efficient in terms of ductility and energy dissipation capacity. Hence, LRS-FRP outside and SRS-FRP inside sequence for H-CFFT is not tested.

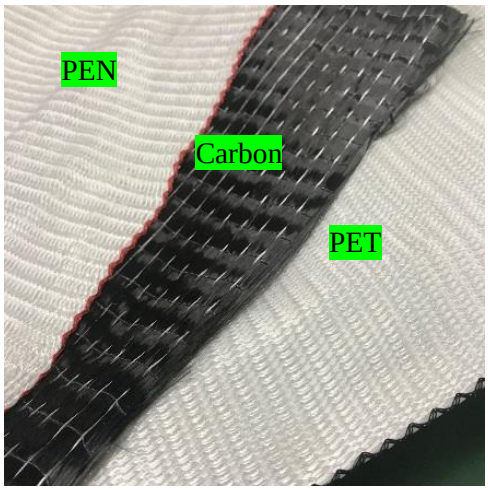

Fig. 1: Types of FRP used in the experiment

3.1. FRP TUBES PREPARATION

The FRP tubes were fabricated using manual wet layup procedure with a 30% overlap length of the tube's perimeter (Fig. 2). The fiber was impregnated with the epoxy using a roller and wrapped around a sonotube. The excess epoxy was squeezed out and cured for 24 hours at room temperature. After curing, sonotube was removed, and a hollow cylindrical FRP tubes was produced. Tyfo® S epoxy having two components A and B were used in the process.

3.2. FRP COUPON TENSILE TESTS

To determine the properties of FRP, flat FRP coupons were prepared and tested (Fig. 3 and Table. 2). FRP plates were prepared in starting using same FRP material and curing procedure, and flat FRP coupons were cut from those FRP plates. All the coupons

Table 1: Tested CFFTs

	Cylinder label	FRP type	FRP plies #			Total FRP plies thickness [mm (inch)]	Confinement ratio (CR)
			PET	PEN	CFRP		
LRS-CFFT	P1	PET	1	-	-	3.3 (0.13)	0.15
	P2		2	-	-	6.6 (0.26)	0.29
	P3		3	-	-	9.9 (0.39)	0.44
	P4	PEN	-	1	-	3.0 (0.12)	0.19
	P5		-	2	-	6.0 (0.24)	0.37
	P6		-	3	-	9.1 (0.36)	0.56
SRS-CFFT	C1	CFRP	-	-	1	0.76 (0.03)	0.23
	C2		-	-	2	1.78 (0.07)	0.46
	C3		-	-	3	2.54 (0.10)	0.69
H-CFFT	C4	PET-CFRP (in/out)	1	-	2	5.08 (0.20)	0.61
	C5	PEN-CFRP (in/out)	-	1	2	4.78 (0.19)	0.65
	C6		-	2	1	6.76 (0.27)	0.60

Fig. 2: Fabricated Hollow Cylindrical FRP tubes

were 254 mm (10 inches) long and 25.4 mm (1 inch) wide. Each end of the coupon was tabbed using aluminum tabs. Strain gauges in the middle and extensometer were used to calculate strain. Three identical coupons of each FRP were prepared. The coupons were tested using MTS 880 at loading rate of 0.5 inches/minute.

LRS-FRP coupons show bilinear stress-strain relationship whereas SRS-FRP coupons show linear stress-strain relationship up to rupture (Fig. 4). In case of LRS-FRP coupons, failure is observed due to longitudinal slippage between the fibers and in case of SRS-FRP coupons, rupture of the FRP at mid-height is observed.

3.3. CONCRETE MIX

Concrete was poured inside the hollow FRP tubes and cured for 28 days at laboratory ambient temperature 29°C (84.20°F). The CFFT specimens were poured in one batch using the concrete mixture shown in Table 3 (Nain et al. 2017). The average 28-day compressive strength of the three number of concrete cylinders was determined per ASTM C39 as 50.3 MPa (7.3 ksi) with a standard deviation of 0.31 ksi.

4. TEST PROCEDURE AND LOADING PROTOCOL

For each CFFT, four axial and hoop strain gauges were installed at the mid-height of the CFFT. First strain gauge was installed within the overlapping zone and other three were symmetrically distributed and evenly placed at 90° outside the overlapping zone. Moreover, additional four hoop strain gauges were symmetrically installed in between the existing strain gauges (Figs. 5 and 6 (a)). In addition, two linear variable displacement transducers (LVDTs) at 180° were installed to measure axial displacement along total height (Fig. 6 (b)).

(a)

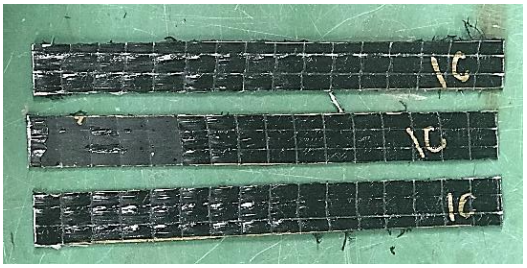

(b)

(c)

Fig. 3: FRP coupons (a) LRS, (b) SRS, and (c) H-FRP

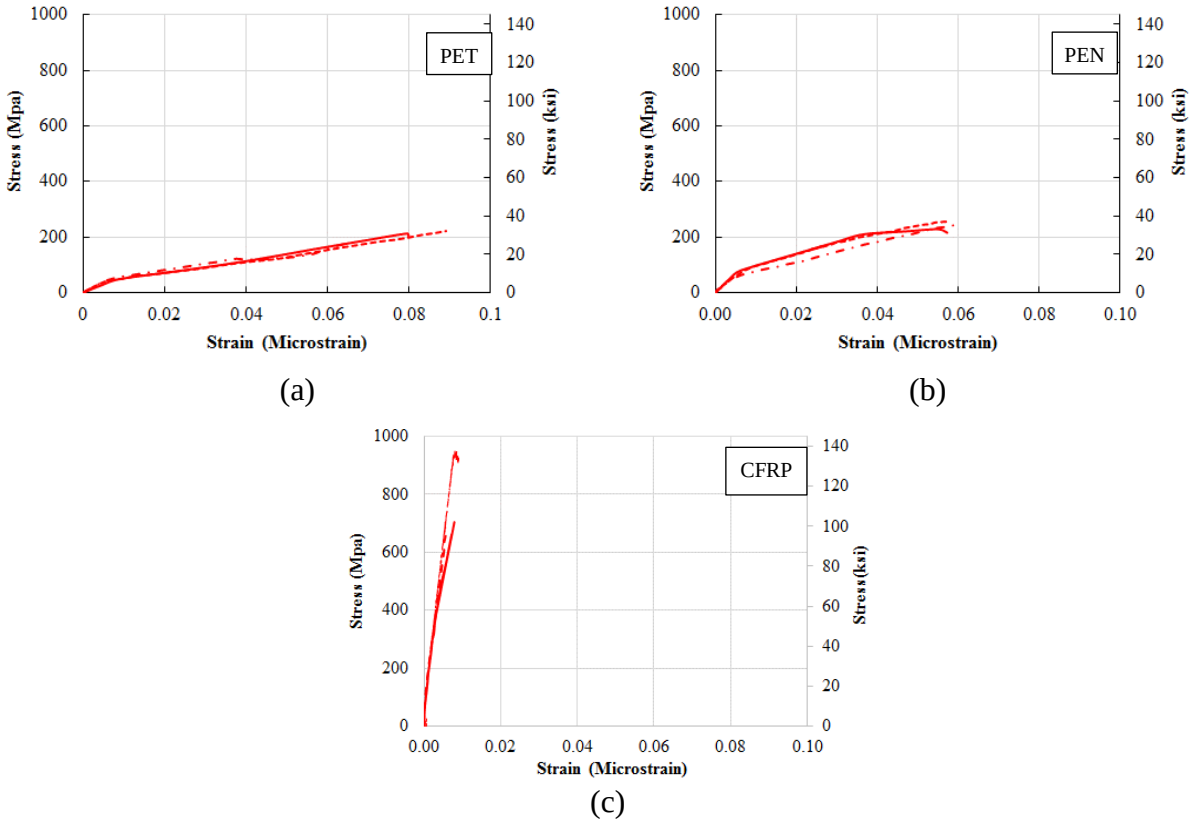

Fig. 4: FRP coupons tensile test results (a) PET, (b) PEN, and (c) CFRP

Table 2: Results of Flat Coupon Test of FRP

Properties	Carbon	PET	PEN
Thickness/ply [mm (inch)]	0.76 (0.03)	3.3 (0.13)	3.0 (0.12)
E [GPa (ksi)]	111.5 (16,179)	2.4 (348)	3.9 (449.6)
Ultimate strain (%)	0.8±0.01	7.7±0.01	5.7±0.01

Table 3: Concrete Mix

w/c	Cement [kg/m^3 (lb/ft^3)]	Water [kg/m^3 (lb/ft^3)]	Fine aggregate [kg/m^3 (lb/ft^3)]	Coarse aggregate [kg/m^3 (lb/ft^3)]
0.5	451 (28.15)	226 (14.1)	512 (32)	512(32)

The cylinders were subjected to cyclic axial compression loading until rupture of the FRP or reaching the ultimate load of the testing machine (Fig. 7). All CFFTs tests were carried out using an MTS 2500 having capacity of 2,400 kN (539 kips) with displacement control at a rate of 0.5 mm/minute (0.02 inch/minute). The CFFTs were first preloaded to 44.5 kN (10 kips). Each loading step was repeated for three cycles (Carter et al. 2014). A data logger system was used to record all the test data, including strains, loads, and displacements.

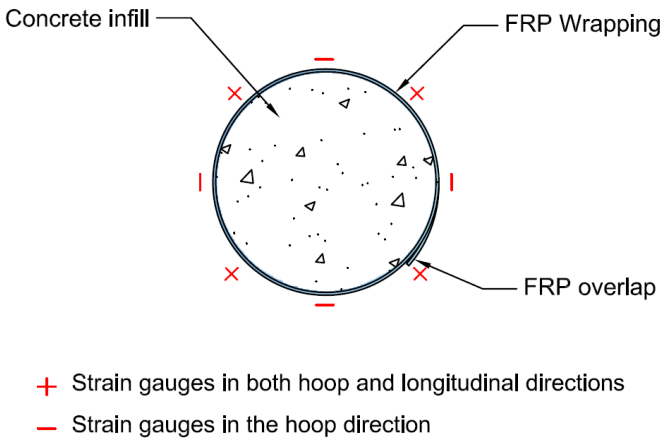

Fig. 5: Positions of the mounted strain gauges

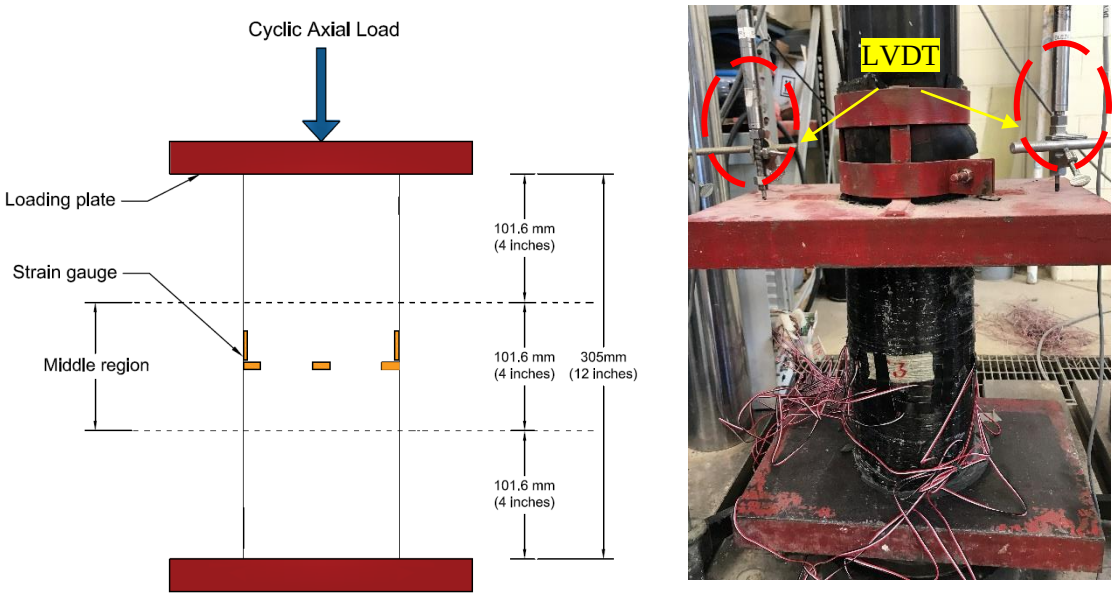

Fig. 6: The CFFT (a) Schematic, and (b) CFFT Test in progress

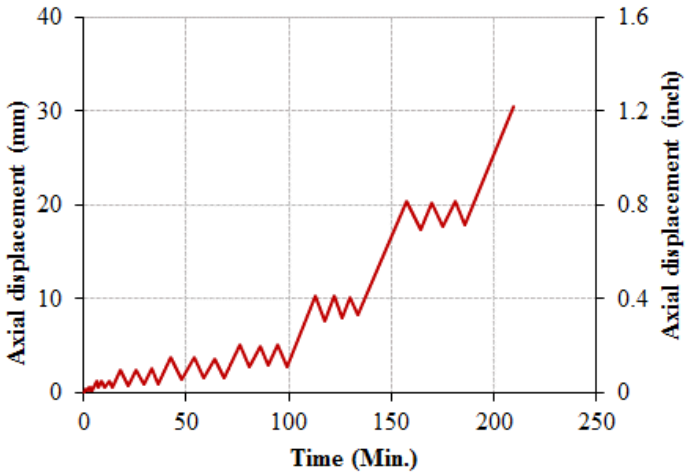

Fig. 7: Cyclic compression loading protocol (Carter et al. 2014)

5. TEST RESULTS

5.1. GENERAL BEHAVIOR

CFFT were experimentally tested under cyclic axial compression and results were discussed in terms of confinement effectiveness, ductility, dilation properties and energy dissipation. Table 4 represents the results of the tested CFFTs in terms of ultimate load capacity P_{max}, displacement, ultimate axial strain (ε_{lu}), and ultimate hoop strain (ε_{hu}). Average of the two LVDTs were used to calculate axial strains. However, strain gauges data were used to calculate hoop strains at mid-height. H-CFFT shows the same strength enhancement as LRS-PET-CFFT and SRS-CFFT. It is worth noting that the capacity of specimens P6, P10, and P12 exceeded the capacity of the MTS compression machine, so the specimens were not tested until complete rupture of the FRP.

5.2. FAILURE MODE

Typical failures of the tested CFFTs' are represented in Figs. 8 to 12. All the LRS-CFFTs' failed by the rupture of the FRP in the hoop direction (Figs. 8 and 9). LRS-PET-CFFT failed at the overlap location (Fig. 8) whereas none of the LRS-PEN-CFFTs failed at overlap location (Fig. 9). The rupture of FRP were concentrated in the central zone of CFFT.

The failure of SRS-CFFTs' was dominated by the rupture of the FRP in the hoop direction (Fig. 10) either in the central zone or in the entire height of tube. Due to higher stiffness of CFRP, the rupture of CFFT was sudden with loudly noise as compared to LRS-CFFT. It is worth to mention that no rupture of FRP is observed in the case of 3-layers PEN and 3-layers CFRP-CFFTs' as MTS loading cell reached the ultimate capacity.

Table 4: Test CFFTs and Key Test Results

	Cylinder label	FRP Parameter	P_{max} [kN (kip)]	Ultimate displacement [mm (inch)]	Ultimate axial strain (ε_{lu}) (%)	Ultimate hoop strain (ε_{hu}) %
LRS-CFFT	P1	PET	1,227 (276)	26.4 (1.04)	8.6	2.2
	P2		1,649 (371)	32.9 (1.30)	11.1	2.3
	P3		2,369 (533)	38.4 (1.50)	12.6	2.8
	P4	PEN	1,409 (317)	15.5 (0.60)	5.1	1.05
	P5		2,072 (466)	16.1 (0.60)	5.3	1.10
	P6		2,384 (536)*	19.4 (0.76)*	6.3*	0.85*
SRS-CFFT	C1	CFRP	1,744 (392)	7.12 (0.28)	1.1	0.83
	C2		2,255 (507)	9.4 (0.37)	1.5	0.95
	C3		2,371 (533)*	8.3 (0.34)*	1.9*	0.45*
H-CFFT	C4	PET-CFRP (in/out)	2,384 (536)*	15.2 (0.60)*	2.5*	0.47*
	C5	PEN-CFRP (in/out)	2,384 (536)*	7.62 (0.30)*	2.1*	0.41*
	C6		2,349 (528)	19.3 (0.76)	7.3	0.91

* *MTS machine exceeded the allowable capacity*

The failure modes of the H-CFFTs are shown in Fig. 11. For 1 PET/2 CFRP (Fig. 11(a)), failure occurred due to rupture of SRS-FRP. The orientation of final rupture is diagonal initiated by hoop rupture of SRS-FRP. For 1 PEN/2 CFRP (Fig. 11(b)), no rupture is observed and MTS machine reached the capacity of loading cell before failure. For 2 PEN/ 1 CFRP (Fig. 11(c)), hoop rupture of SRS-FRP in the central zone was observed similar to LRS-CFFTs and SRS-CFFTs.

(a) (b) (c)

Fig. 8: PET-CFFTs after failure (a) P1 (1 layer), (b) P2 (2 layer), and (c) P3 (3 layer)

(a) (b) (c)

Fig. 9: PEN-CFFTs after failure (a) P4 (1 layer), (b) P5 (2 layer), and (c) P6 (3 layer)

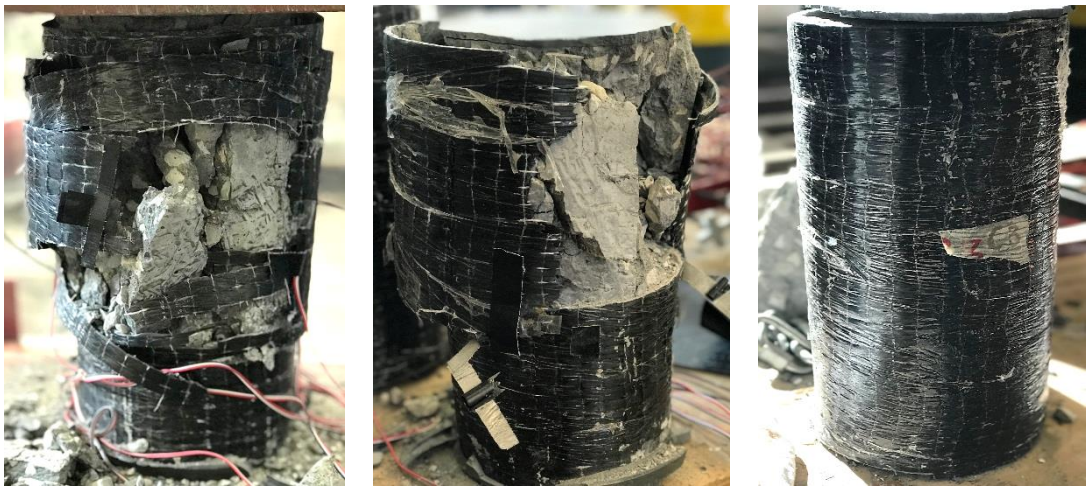

(a) (b) (c)

Fig. 10: CFRP-CFFTs after failure (a) C1 (1 layer), (b) C2 (2 layer), and (c) C3 (3 layer)

(a) (b) (c)

Fig. 11: H-CFFT after failure [in/out] (a) C4 (1 PET/2 CFRP), (b) C5 (1 PEN/2 CFRP), and (c) C6 (2 PEN/1 CFRP)

5.3. AXIAL STRESS-STRAIN RESPONSE

Normalized stress-strain curves of cyclically tested CFFTs are shown in Figs. 12 to 16. Axial strain and hoop strain are represented by positive and negative x-axis respectively.

The normalized stress-strain behavior of LRS-PET FRP tubes (P1, P2, and P3) is represented in Fig.12. CFFTs' exhibit an ascending first branch with an increase of 40-150 % in confined strength capacity depending upon number of FRP layers used. The stress-strain behavior in second branch was influenced significantly by the amount of confining FRP. Figs. 12 (a) and (b) shows CFFTs P1 and P2 experienced initial strength softening i.e. a sudden drop in strength followed by 40% recovery in strength. This strength drop is associated with the brittle nature of concrete. However, for CFFT P3 (Fig. 12 (c)), the second portion is of a continuously ascending type with an insignificant softening curve. This behavior is associated with sufficient confinement provided by PET-FRP. CFFTs shows ductile behavior with 8-12% of axial strain.

The normalized stress-strain behavior of LRS-PEN FRP tubes (P4, P5, and P6) is represented by Fig. 13. CFFTs exhibit an ascending first branch i.e. similar behavior as of LRS-PET FRP. The first branch of the curve shows an increase of 50%- 150% in confined strength capacity for one to three layers of FRP. The second branch experienced initial strength softening with a strength drop of 10% - 20% and then followed by ascending curve. It is worth to mention that in Fig. 13 (c) (P6), the plateau at the top occurs because the MTS machine loading cell reached its capacity without rupture of the CFFT specimen. CFFTs' shows ductile behavior with 5-6% of axial strain.

The normalized stress-strain behavior of SRS-FRP tubes (C1, C2 and C3) is represented by Fig.14. CFFTs' exhibit an ascending linear curve up to ultimate strength with an increase in confined strength capacity by 100-150%. However, less ductility is achieved with small rupture strain value of 1%. From Fig. 14 (c), plateau at the top represents capacity of MTS machine loading cell reached. No rupture of FRP is observed, it is due to the high stiffness modulus of CFRP.

The normalized stress-strain behavior of H-PET-CFRP (C4) is represented by Fig. 15. The H-CFFT exhibit an ascending linear curve reaching the ultimate capacity of MTS machinne loading cell. The increase in confined strength by 150% is observed with rupture of FRP at 2.5% axial strain.

The normalized stress-strain behavior of H-PEN-CFRP (C5 and C6) is represented by Fig. 16. The H-CFFT exhibit an ascending linear curve reaching the ultimate capacity of MTS machine loading cell (Fig. 16 (a)). The increase in confined strength by 150% is observed. Due to presence of LRS-PEN FRP with CFRP there is increase in ductility of SRS-CFFTs. However, CFFT C6 (Fig. 16 (b)) exhibit ascending first branch followed by descending branch. However, ductility of CFFT is improved with an axial strain of 6%.

To conclude, a hybrid system having 1 LRS FRP/2 CFRP reveals more strength gain due to the higher stiffness of CFRP. Moreover, with the strength gain, ductility is also provided by LRS FRP in both LRS-CFFTs' and H-CFFTs' because of large rupture strain and efficient confinement.

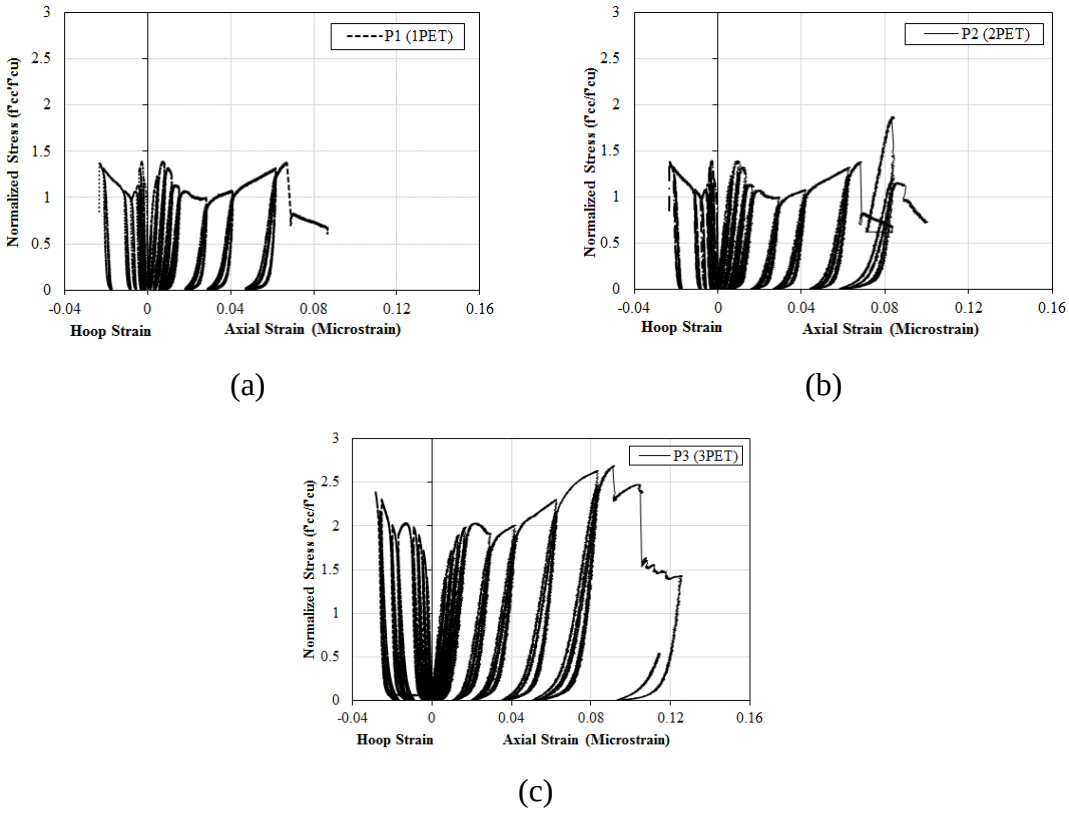

Fig. 12: Normalized Stress via strain curves of PET-CFFTs (a) P1 (1 layer), (b) P2 (2 layers), and (c) P3 (3 layers)

5.4. CONFINEMENT PRESSURE

Under axial compression, CFFT is subjected to lateral confinement provided by the FRP tube. This lateral confinement provides tension in the hoop direction and prevents concrete expansion. Hence, strength and ductility can be increased significantly due to presence of this lateral confinement.

The results of the tested CFFTs' are represented by table 5. The ultimate confinement effectiveness (f'_{cc}/f'_c) where f'_{cc} is the ultimate strength of confined concrete, f'_c is the compressive strength of unconfined concrete i.e. 50.3 MPa (7.3 ksi) and strain

gain with respect to confinement ratio (CR) where ε_{cc} and ε_{cu} (0.13 inch/inch) are the ultimate axial strain of the confined and unconfined concrete; respectively. Fig. 22 shows the relation between confinement effectiveness and confinement ratio.

Table 5 shows that SRS-CFFTs' were more efficient than LRS-CFFTs' in terms of confinement effectiveness. However, both LRS-CFFTs and H-CFFTs shows more ductile behavior irrespective of same confinement ratio.

As shown in Fig 17 (a), for one and two layers of CFFTs, SRS-CFFT shows higher confinement effectiveness of 20%-25% and 13%-50% than LRS-CFFTs respectively.

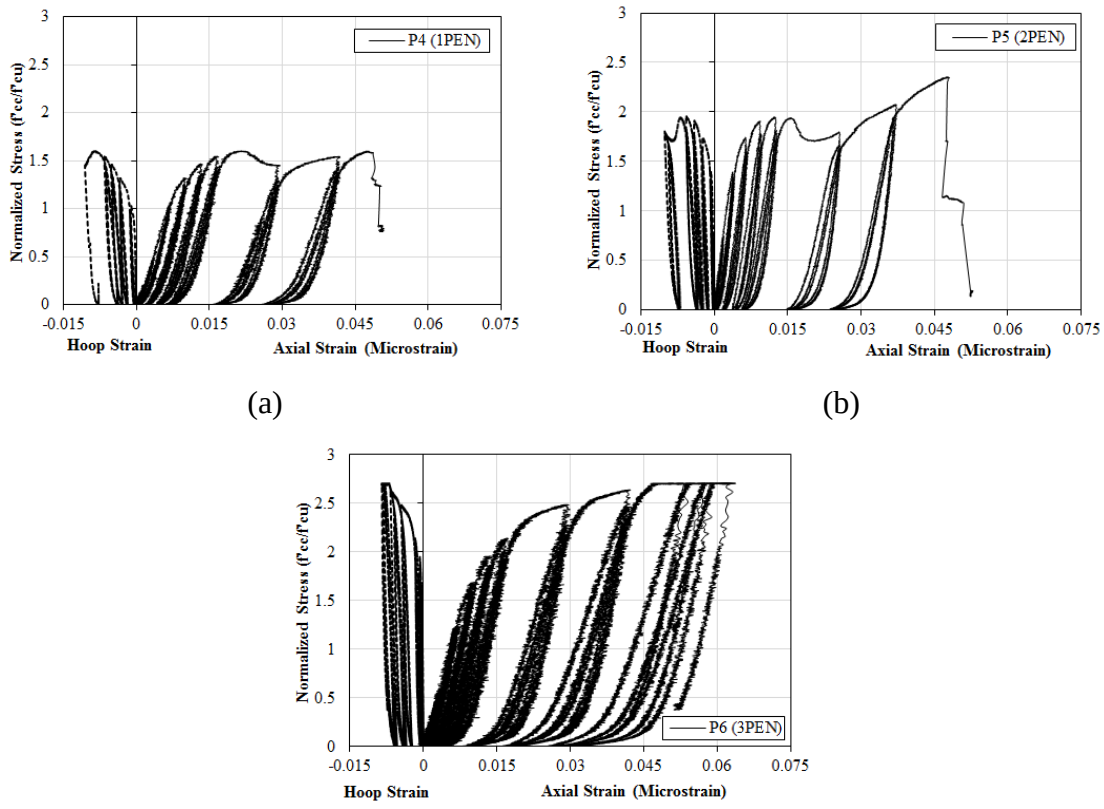

Fig. 13: Normalized Stress via strain curves of PEN-CFFTs (a) P4 (1 layer), (b) P5 (2 layers), and (c) P6 (3 layers)

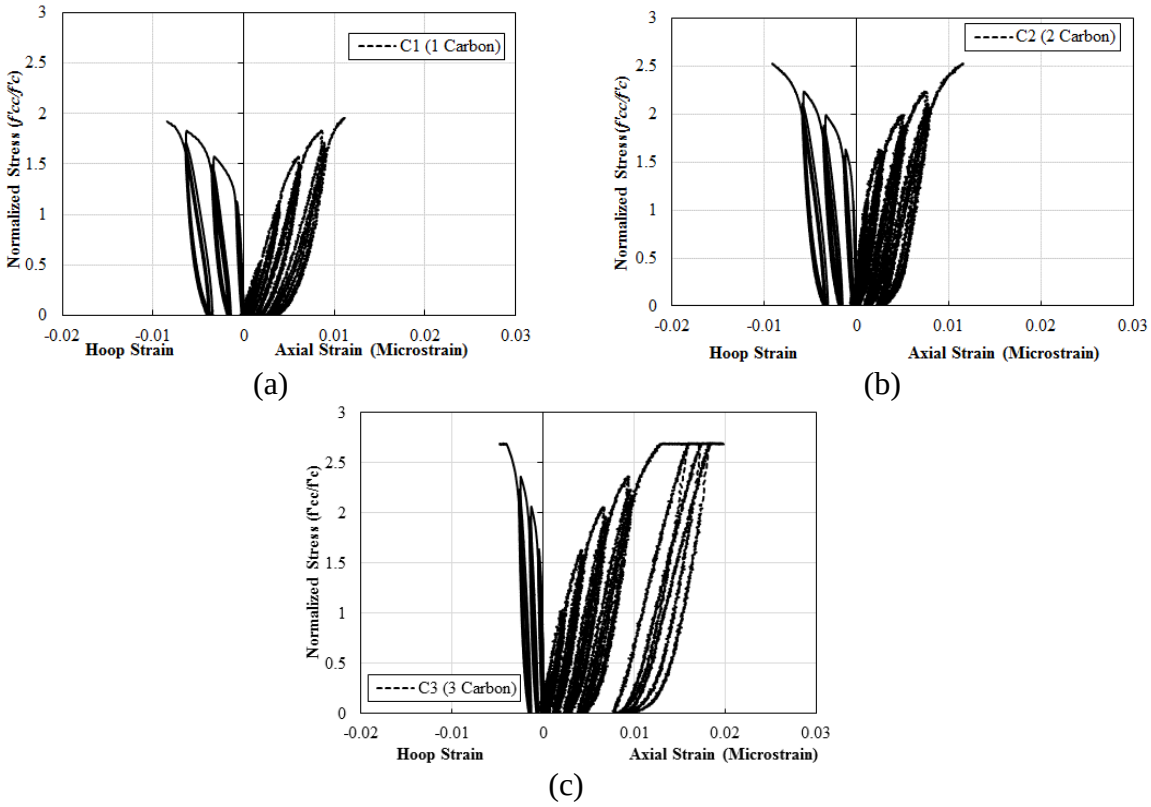

Fig. 14: Normalized Stress via strain curves of CFRP-CFFTs (a) C1 (1 layer), (b) C2 (2 layers), and (c) C3 (3 layers)

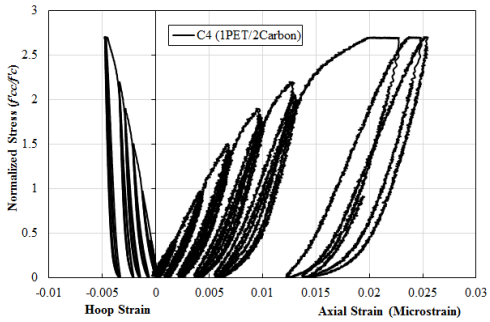

Fig. 15: Normalized Stress via strain curves of H-CFFTs [C4 (1 PET/2 CFRP)]

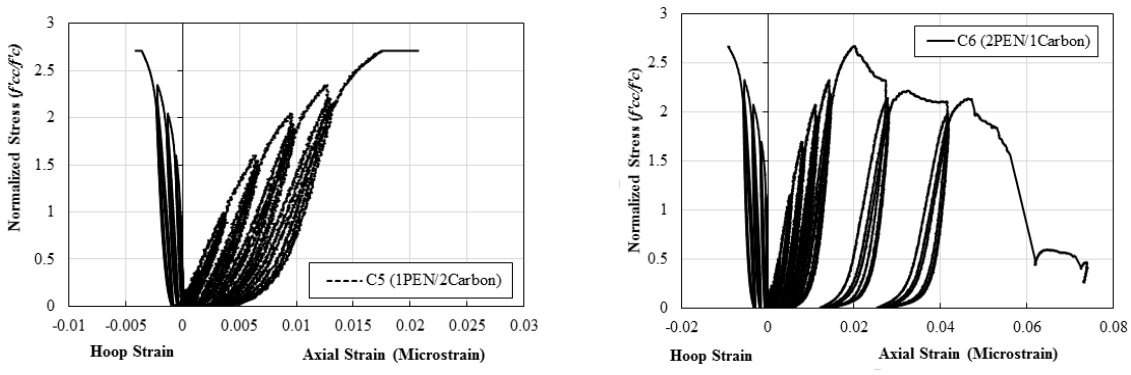

(a) (b)

Fig. 16: Normalized Stress via strain curves of H-CFFTs (a) C5 (1 PEN/2 CFRP), and (b) C6 (2 PEN/1 CFRP)

However, for three layers of FRPs both LRS-CFFTs and SRS-CFFTs performs shows same confinement effectiveness.

From Fig. 17 (a) and Table 5, it can be concluded that LRS-PEN-CFFTs performed better in terms of confinement effectiveness than LRS-PET-CFFTs. However, LRS-PET-CFFTs were more ductile than LRS-PEN-CFFTs. The reason was the higher rupture strain value of PET-FRP (6-8%) than PEN-FRP (4-5%).

Confinement effectiveness via confinement ratio of all the three layers CFFTs i.e. SRS-CFFT, LRS-CFFT, and H-CFFT are represented by Fig. 17 (b). Despite difference in confinement ratios, all tested CFFTs' shows same confinement effectiveness. From Fig. 22, it can be observed that there is a linear increase in the confinement effectiveness for CR range between 0.1-0.4 (Fig.17 (a)) but it is constant for CR above 0.4 (Fig.17 (a)). Hence, LRS-CFFT and H-CFFT shows same strength enhancement as SRS-CFFT but more ductile behavior.

Table 5: Key Test Results of CFFTs

	Cylinder label	f'_{cc} [MPa (ksi)]	Confinement effectiveness (f'_{cc}/f'_c)	ε_{cc} (inch/inc)	$\varepsilon_{cc}/\varepsilon_{cu}$	f_l^{**} [MPa (ksi)]	CR^{***}
LRS-CFFT	P1	67.5 (9.78)	1.39	0.09	6.92	7.1 (1.02)	0.15
	P2	90.3 (13.11)	1.87	0.11	8.46	14.2 (2.05)	0.29
	P3	129.8 (18.84)	2.69	0.13	10.00	21.3 (3.08)	0.44
	P4	77.2 (11.20)	1.60	0.05	3.85	9.1 (1.31)	0.19
	P5	113.5 (16.47)	2.35	0.05	3.85	18.01 (2.6)	0.37
	P6	130.5* (18.94)	2.71	0.06	4.62	27.1 (3.92)	0.56
SRS-CFFT	C1	95.5 (13.86)	1.98	0.011	0.85	7.2 (1.66)	0.23
	C2	123.6 (17.93)	2.56	0.015	1.15	14.9 (3.32)	0.46
	C3	129.9* (18.85)	2.69	0.019	1.46	22.2 (4.98)	0.69
	C4	130.7* (18.96)	2.71	0.025	1.92	22.2 (4.38)	0.61
	C5	130.6* (18.95)	2.71	0.021	1.62	23.6 (4.66)	0.65
	C6	128.7 (18.67)	2.67	0.073	5.62	25.6 (4.34)	0.60

* *MTS machine capacity was reached*

** *Confinement pressure from Eq.2*

****CR: Confinement ratio from Eq.1*

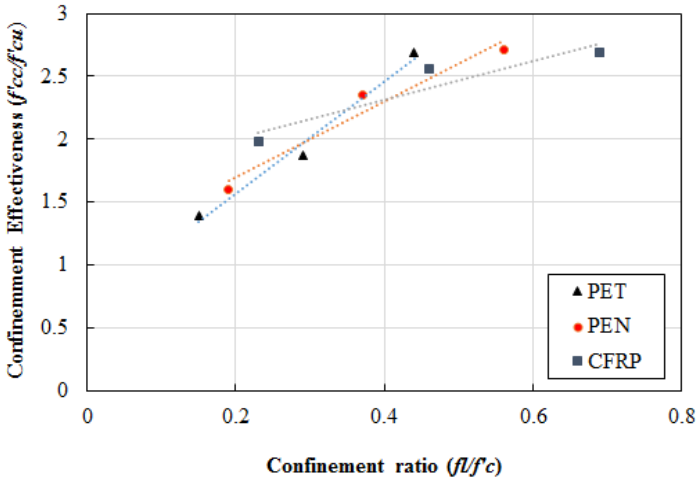

(a)

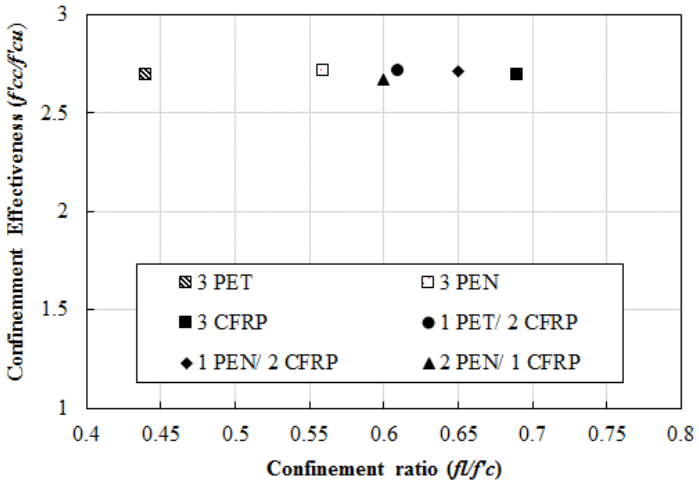

(b)

Fig. 17: Confinement effectiveness vs. confinement ratio of (a) LRS-CFFTs' and SRS-CFFTs' (P1-P6, C1-C3), and (b) all 3 layers CFFTs'

5.5. CONCRETE DILATION BEHAVIOR

It is a well-known phenomenon that unconfined concrete experiences volumetric dilation after initial volume reduction up to 90% of the compressive strength (Chen 2007). This volumetric dilation phenomenon originates from the formation of cracks under axial

stresses. However, in case of the CFFTs, confinement provided by the FRP passively restricts the volume dilation of concrete under compression.

The volumetric strain curves for CFFTs' are represented by Figs.18 to 20. For LRS-PET-CFFTs, the direction got reversed from volume reduction to expansion at 0.9 *f'c,* but in the end concrete failed in compaction (Fig.18 (a)). The reason is the confinement pressure from FRP prevents the expansion of concrete. Failure is controlled by compaction at 1.3 and 1.8 of normalized axial stress reached by P1, P2, and P3 respectively depending on number of FRP layers used.

Depending on the confinement provided by FRP, volume expansion in CFFTs is prevented by FRP at 1.5 normalized axial stress (Fig. 18 (b)) and failed in compaction in case of one and two layers of FRP-CFFTs. For three layers of PEN-CFFT, failed in expansion but direction got reversed from volume reduction to volume expansion after 100% increase in normalize stress.

For SRS-CFFTs', due to presence of insufficient confinement CFFT got failed in expansion (Fig.18 (c)). However, for three layers of SRS-FRP volume expansion is curtailed by FRP up to 250% of normalized stress (Fig. 18 (c)). The reason is high confinement pressure provided by FRP.

For H-CFFTs', absence of volume expansion is observed in case of 1LRS-2SRS-CFFTs up to 250% increase in the normalized stresses (Fig. 19 and 20) However, in case of 2LRS-1SRS-CFFTs expansion after increase of 50% in stress is observed (Fig. 20). The reason could be the higher stiffness available due to presence of two layers of SRS-FRP.

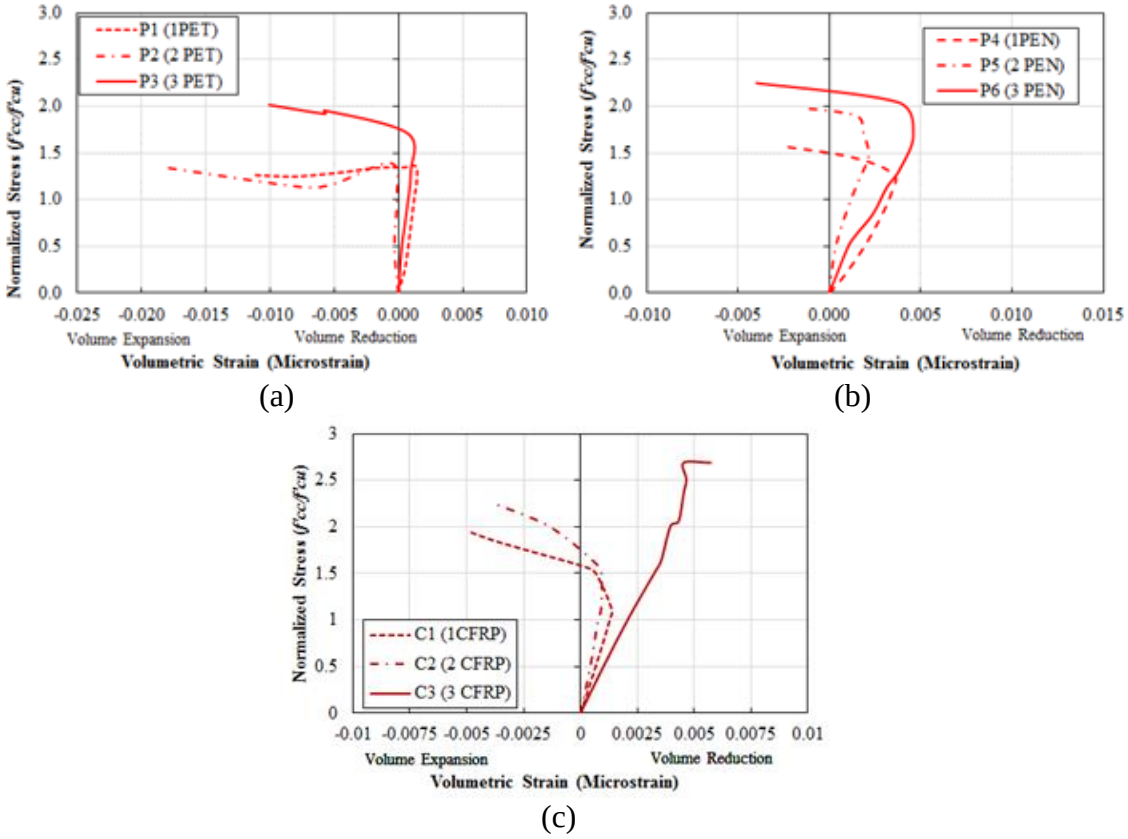

Fig. 18: Volumetric Strain curves of CFFTs (a) PET-CFFTs, (b) PEN-CFFTs, and (c) CFRP-CFFTs

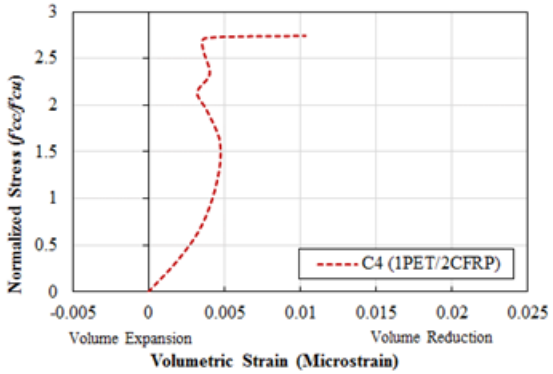

Fig. 19: Volumetric Strain curves of H-CFFTs: C4 (1 PET/2 CFRP)

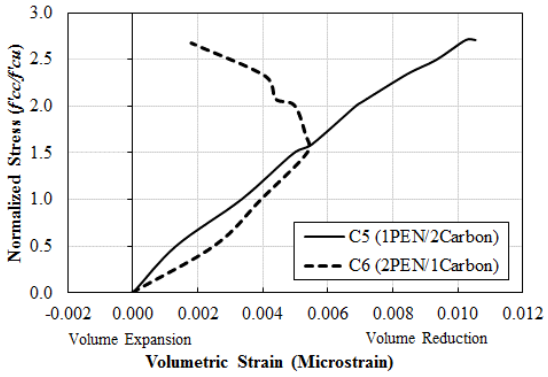

Fig. 20: Volumetric Strain curves of H-CFFTs: PEN/CFRP

5.6. ENERGY DISSIPATION CAPACITY

Energy dissipation capacity is one of the most important crucial parameter in seismic design criteria for a structure. Cumulative energy dissipation can be calculated by summing up the dissipated energy for the first cycle in successive load-displacement cycle. Figs. 21 to 23 show the cumulative energy dissipation capacity of tested CFFTs.

From Fig. 21, it can be observed that LRS-CFFTs energy dissipation capacity is significant. The reason for this significant energy dissipation capacity is the large rupture strain value which provides ductility to the system. However, SRS-CFFTs have lower value of energy dissipation capacity (Fig. 22). The reason is smaller rupture strain value and high stiffness value of CFRP. It can be concluded that LRS-CFFTs' shows an efficient system to be used in seismic areas as energy dissipation capacity of LRS-FRP is significant.

Fig. 23 shows the energy dissipation capacity of H-CFFT. It can be observed that 1 LRS-2 SRS-CFFT has higher energy dissipation capacity than 3-SRS-CFFT. It is worth to mentioned, that 1 PEN- 2 CFRP-CFFT (Fig. 23 (a)) reached the ultimate capacity without failure of FRP rupture. Moreover, 2 PEN-1 CFRP-CFFT (Fig. 23 (b)) has also

improved the energy dissipation capacity of SRS-CFFT. Hence, by H-CFFT energy dissipation capacity of SRS-CFFTs can be improved by significant amount. However, LRS- CFFT are better efficient system that H-CFFT and SRS-CFFT.

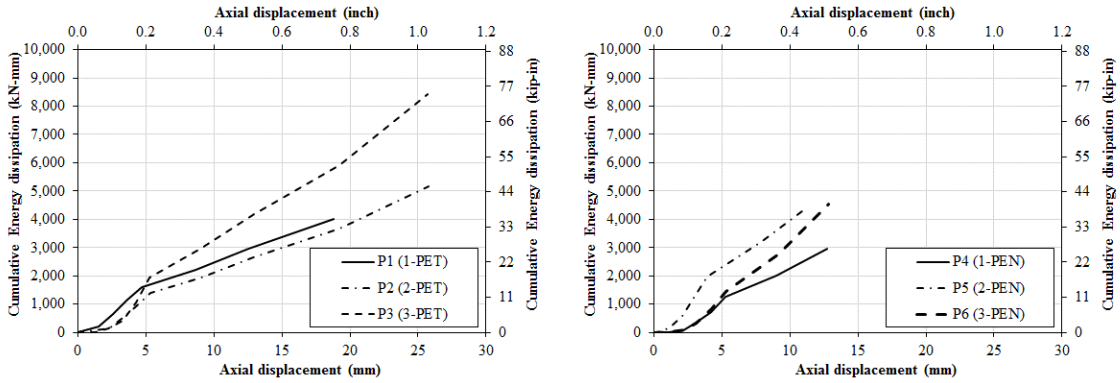

(a) (b)

Fig. 21: Cumulative energy dissipation via axial displacement of LRS-CFFTs (a) PET-CFFTs, and (b) PEN-CFFTs

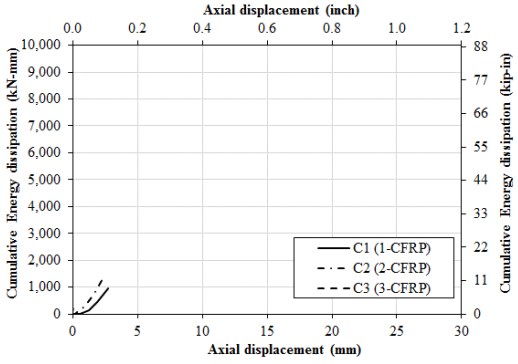

Fig. 22: Cumulative energy dissipation via axial displacement of SRS-CFFTs, CFRP-CFFTs

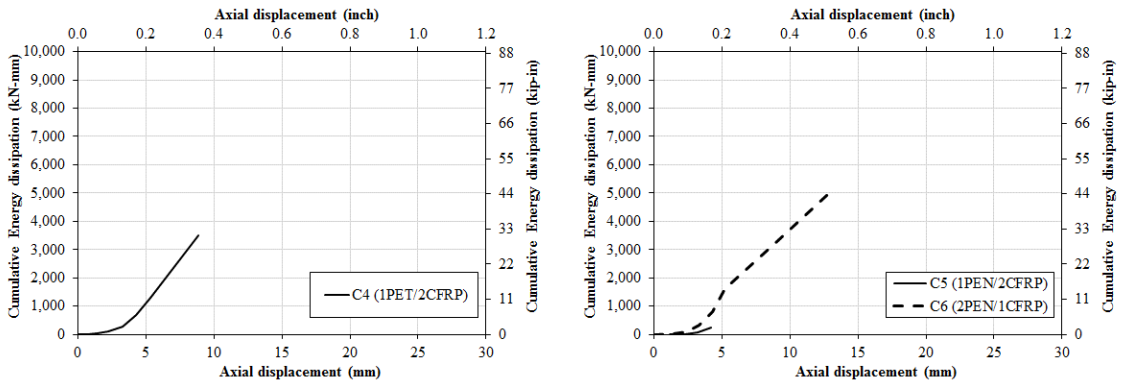

(a) (b)

Fig. 23: Cumulative energy dissipation via axial displacement of H-CFFTs (in/out) (a) PET-C-CFFT, and (b) PEN-C-CFFT

5.7. COMPARISON WITH EXISTING MODELS

The ultimate compressive strength obtained from the tested CFFTs are compared with the present confinement models. Models used in this study are: Saafi et al. (1999), Shehata et al. (2002), Ilki and Kumbasar (2003), Shao et al. (2006), and Teng et al. (2009) (Table 6).

Fig. 24 shows the ratio of analytical compressive strength and test compressive strength via (a) confinement ratio, and (b) test compressive strength. Table 7 shows the statistical result of the evaluated analytical models having average, standard deviation (SD), coefficient of variation (COV), and number of overestimated CFFTs.

From Fig. 24 (a) and table 7, it can be observed that Shao el al. (2006) and Teng et al. (2009) models have estimated the strength most accurate for C.R. having values lesser than 0.50. However, for C.R. having values greater than 0.50, Teng et al. has overestimated the strength whereas Shao et al. has underestimated the strength. Shehata et al. (2002) and

Ilki et al. (2003) underestimated the strength by 10%-30%. This same results were oberved with SRS-Glass-CFFTs and H-CFFTs with glass FRP. Therefore, no model exactly predict the behavior of CFFTs with higher C.R.

Table 6: Available analytical confinement models

Model	Confined Compressive Strength	Confinement pressure f_l	
(Saafi et al. 1999)	$\frac{f'_{cc}}{f'_{co}} = 1 + 2.2(\frac{f_l}{f'_{co}})^{-0.16}$	$f_l = \frac{2f_f n t_f}{D}$	(4)
(Shehata et al. 2002)	$\frac{f'_{cc}}{f'_{co}} = 1 + 2.0\frac{f_l}{f'_{co}}$	$f_l = \frac{2f_f n t_f}{D}$	(5)
(Ilki and Kumbasar 2003)	$\frac{f'_{cc}}{f'_{co}} = 1 + 2.23\frac{f_l}{f'_{co}}^{0.7}$	$f_l = \frac{f_f \rho_f}{2}$ $\rho_f = \frac{4nt_f}{D}$	(6)
(Shao et al. 2006)	$\frac{f'_{cc}}{f'_{co}} = 1 + 6\frac{f_l}{f'_{co}}$	$f_l = \frac{2f_f n t_f}{D}$	(7)
(Teng et al. 2009)	$\frac{f'_{cc}}{f'_{co}} = 1 + 3.5\frac{f_{le}}{f'_{co}}$	$f_{le} = \frac{\varepsilon_{fe} E_f n t_f}{R}$	(8)

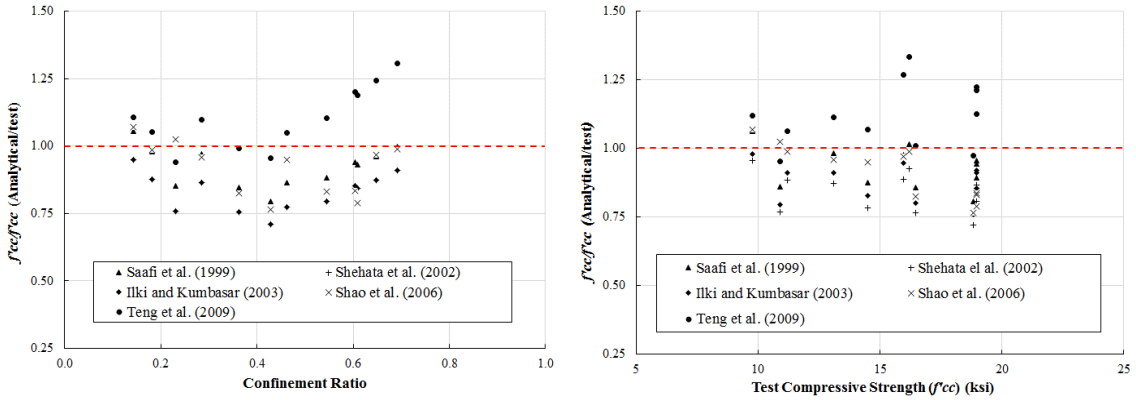

(a) (b)

Figure 24: Ratio of analytical compressive strength and test compressive strength via (a) confinement ratio, and (b) test compressive strength

Table 7: Statistical result of the evaluated analytical models

Model	Average	Standard Deviation	COV	# over estimated CFFTs'
Saafi et al. (1999)	0.96	0.08	0.09	2
Shehata et al. (2002)	0.87	0.08	0.10	0
Ilki and Kumbasar (2003)	0.91	0.08	0.09	0
Shao et al. (2006)	0.93	0.09	0.09	2
Teng et al. (2009)	1.17	0.13	0.11	10

6. CONCLUSION

In this paper, an experimental study was investigated to explain the cyclic compressive behavior of concrete confined to large rupture strain FRP (LRS-FRP) or hybrid LRS-FRP and CFRP (SRS-FRP). Twelve cylinders were tested for different confinement ratio. The study concluded the following notes.

1. LRS-FRP is more ductile than SRS-FRP with same strength enhancement as of CFRP.
2. Between LRS-FRP, PET-FRP has better performance than PEN-FRP in terms of ductility, and energy dissipation capacity.
3. H-CFFT improves the ductility of SRS-FRP with same strength enhancement. However, LRS-FRP performs better than H-CFFT in terms of strength, ductility.
4. In terms of energy dissipation, LRS-CFFTs' and H-CFFTs' both are efficient than SRS-CFFTs.

Finally, LRS-CFFTs is a promising system for improved ductility and strength of concrete-filled FRP tubes. In seismic areas, it can be an effective system due to its ductility and energy dissipated capacity. Moreover, ductility and energy dissipation capacity.

REFERENCES

Abdelkarim, Omar I., and Mohamed A. ElGawady. "Concrete-filled-large deformable FRP tubular columns under axial compressive loading." *Fibers3*, no. 4 (2015): 432-449.

Bai, Y.-L., Dai, J.-G., and Teng, J. (2013). "Cyclic compressive behavior of concrete confined with large rupture strain FRP composites." Journal of Composites for Construction, 18(1), 04013025.

Bai, Y. (2014). "Behavior and modeling of RC columns confined with large-rupture strain FRP composites." The Hong Kong Polytechnic University.

Carter, J., Abdelkarim, O., ElGawady, M., and Khayat, K. (2014) "FRP Confinement of High Strength Self-Consolidating Concrete." Proc., 10th US National Conf. on Earthquake Engineering, Alaska, USA.

Choi, K.-K., and Xiao, Y. (2009). "Analytical model of circular CFRP confined concrete-filled steel tubular columns under axial compression." *Journal of Composites for Construction*, 14(1), 125-133.

Dai, J.-G., and Ueda, T. (2012). "Strength and deformability of concrete members wrapped with fibre-reinforced polymer composites with a large rupture strain." Innovative materials and techniques in concrete construction, Springer, 225-241.

Dawood, H. M., and ElGawady, M. (2013). "Performance-based seismic design of unbonded precast post-tensioned concrete filled GFRP tube piers." Composites Part B: Engineering, 44(1), 357-367.

Fanggi, B. A. L., and Ozbakkaloglu, T. (2013). "Compressive behavior of aramid FRP–HSC–steel double-skin tubular columns." *Construction and Building Materials*, 48, 554-565.

Jirawattanasomkul, T., Dai, J.-G., Zhang, D., Senda, M., and Ueda, T. (2013). "Experimental study on shear behavior of reinforced-concrete members fully wrapped with large rupture-strain FRP composites." Journal of Composites for Construction, 18(3), A4013009.

Mirmiran, A., and Shahawy, M. (1997). "Behavior of concrete columns confined by fiber composites." Journal of Structural Engineering.

Nain, M., Abdulazeez, M. M., and ElGawady, M. A. (2017) "Behavior of Concrete-Filled Hybrid Large Rupture Strain FRP Tubes Under Cyclic Axial Compression." *Proc., Congrès International de Géotechnique–Ouvrages–Structures*, Springer, 346-353.

Ozbakkaloglu, T., Lim, J. C., and Vincent, T. (2013). "FRP-confined concrete in circular sections: Review and assessment of stress–strain models." *Engineering Structures*, 49, 1068-1088.

Rousakis, T. C. (2013). "Elastic fiber ropes of ultrahigh-extension capacity in strengthening of concrete through confinement." Journal of Materials in Civil Engineering, 26(1), 34-44.

Saleem, S., Pimanmas, A., and Rattanapitikon, W. (2018). "Lateral response of PET FRP-confined concrete." Construction and Building Materials, 159, 390-407.

Seible, F., Priestley, M. N., Hegemier, G. A., and Innamorato, D. (1997). "Seismic retrofit of RC columns with continuous carbon fiber jackets." Journal of composites for construction, 1(2), 52-62.

Shao, Y. (2003). "Behavior of FRP-concrete beam-columns under cyclic loading."

Spoelstra, M. R., and Monti, G. (1999). "FRP-confined concrete model." Journal of composites for construction, 3(3), 143-150.

Wu, Y.-F., and Wei, Y.-Y. (2010). "Effect of cross-sectional aspect ratio on the strength of CFRP-confined rectangular concrete columns." *Engineering Structures*, 32(1), 32-45.

SECTION

2. SUMMARY, FINDINGS AND FUTURE WORK RECOMMENDATIONS

2.1. SUMMARY AND FINDINGS

The applications of FRP composites in the civil engineering field had increased and resulted new and different types of FRP materials to meet the structural requirements. The thesis presented the experimental study on cyclic compressive behavior of three types of concrete-filled FRP tubes namely SRS-CFFTs, LRS-CFFTs, and H-CFFTs. FRPs were categorized into two groups such as SRS-FRP having Glass and Carbon-FRP, and LRS-FRP having PET and PEN-FRP.

Results of this experimental study were also compared with existing analytical models to predict the compressive strength of CFFTs. The study concluded the following notes.

1. SRS-CFFTs increase the compressive strength of unconfined concrete by 1.5-2.5. However, SRS-CFFTs shows less ductile behavior.
2. The energy dissipation capacity of SRS-CFFTs is significantly small.
3. LRS-CFFTs show same strength enhancement as of SRS-CFFTs but high ductile behavior with significant energy dissipation capacity.
4. H-CFFTs show similar increase in strength as of SRS-CFFTs and LRS-CFFTs having greater ductility and energy dissipation capacity than SRS-CFFTs.
5. LRS-CFFTs performs better than H-CFFTs.

In seismic regions, LRS-CFFTs can be a promising system in terms of ductility and energy dissipation capacity. Evaluation of experimental results and analytical models show

Teng et. al. and Shao et. al. models predicted well for CFFTs having lower C.R. However, no model was able to predict the strength of CFFTs having large C.R.

2.2. FUTURE WORK RECOMMENDATIONS

The compressive behavior of different types of CFFTs were experimentally investigated. However, a few further investigations were recommended to investigate.

1. The significance of bond between concrete and FRP need to be studied
2. Effect of overlapping length of FRP on failure mode
3. Finite model for H-CFFT to be evaluated
4. The large-scale investigation on H-CFFT was necessary to study different parameters.

VITA

Monika Nain was born in Delhi, India. In 2016, she received her Bachelor Engineering (B.E) degree in Civil Engineering from Deenbandhu Chhotu Ram University of Science and Technology, India. In May 2018, she received her Master of Science (M.S) degree in Civil Engineering with Structural as emphasis from Missouri University of Science and Technology, Rolla, USA.